

ABSTRACT

Dynamic Low Rank (DLR) methods are a promising way to reduce the computational cost and memory footprint of the high-dimensional thermal radiative transfer (TRT) equations. The TRT equations are a system of nonlinear PDEs that model the energy exchange between the material temperature $T(\mathbf{x}, t)$ and the radiation energy density $\psi(\mathbf{x}, \Omega, t)$ at spatial point $\mathbf{x} \in \mathbb{R}^3$ and traveling in direction $\Omega \in \mathbb{S}^2$ at time t ; due to their high dimensionality, solving the TRT equations is often bottleneck in multi-physics simulations. DLR methods represent the solution $\psi(\mathbf{x}, \Omega, t)$ in terms of time-evolving SVD-like factors $W_j(\Omega, t)$ and $X_j(\mathbf{x}, t)$ of angle and space. Although previous work has explored DLR methods for TRT, most of the methods have limitations that make them impractical for realistic scenarios and uncompetitive with current non-DLR production codes.

Here we develop new PN-like and SN-like Dynamic Low Rank (DLR) methods for TRT. In the SN-like DLR method, we use the time-evolving angular basis functions $W_i(\Omega, t)$ to select time-evolving angles $\Omega^{(i)}(t) \in \mathbb{S}^2$; this DLR formulation enables us to use the highly optimized SN transport sweep as our main computational kernel, and results in a practical way of leveraging low-rank methods in production TRT codes. In contrast, our PN-like DLR method uses an even-parity formulation and results in positive-definite linear systems to solve for each time step.

We demonstrate the methods on several challenging, highly heterogeneous problems in two spatial dimensions (4D) that these DLR schemes can give significant reduction in angular artifacts (“ray effects”) with the same cost as gold-standard SN methods.

1. Introduction

Dynamic Low Rank (DLR) methods ([19], [14], [12]) are a promising approach for reducing the computational cost and memory footprint of thermal radiative transfer.

We apply the DLR method to compute the time-dependent photon energy distribution $\psi(\mathbf{x}, \Omega, t)$ of the time-dependent thermal radiative transfer (TRT) equations (see equations (1)-(3)); here $\psi(\mathbf{x}, \Omega, t)$ represents the radiation energy density at spatial point $\mathbf{x} \in \mathcal{X} \subset \mathbb{R}^3$, traveling in direction $\Omega \in \mathbb{S}^2$, at time t . The DLR method represents the solution in terms of a dynamically evolving low-rank representation [14] with rank r_0 ,

$$\psi(\mathbf{x}, \Omega, t) = \sum_{i,j=1}^{r_0} X_i(\mathbf{x}, t) S_{ij}(t) W_j(\Omega, t),$$

where the r_0 spatial basis functions $X_i(\mathbf{x}, t)$ and angular basis functions $W_j(\Omega, t)$ evolve in time to achieve a (nearly) optimally small equation residual for a prescribed solution rank r_0 . The memory footprint for storing $X_i(\mathbf{x}, t)$ and $W_j(\Omega, t)$ scales like $\mathcal{O}(r_0(N_x + N_\Omega))$ and the computational cost scales like $\mathcal{O}(r_0^2(N_x + N_\Omega))$, with N_x and N_Ω denoting the number of spatial and angular unknowns needed to resolve the solution. In contrast, direct numerical discretization schemes require $\mathcal{O}(N_x N_\Omega)$ memory and computational costs. Therefore, when $r_0^2 \ll \max(N_x, N_\Omega)$, DLR offers significant computational savings.

There is a growing literature on applying DLR in the context of both linear transport and (nonlinear) thermal radiative transfer. These include conservative high-order low-order methods for radiative transfer (cf. [28], [13], [11], [3]), as well as sweep-based methods on structured meshes (cf. [31], [29], [30]). Many DLR schemes for kinetic equations such as TRT ensure that key asymptotic-preserving properties hold (cf. [6], [15]).

For TRT applications, there are still outstanding challenges for making DLR practical in realistic scenarios compared to a gold-standard deterministic method like the discrete-ordinates (SN) method. One major challenge is that the number N_Ω of angular collocation points needed for acceptable physics fidelity in SN simulations can be quite small

ORCID(s):

in practice compared to the number of spatial unknowns N_x ; in fact, radiation hydrodynamics simulations typically use the hydrodynamics mesh to represent the spatial unknowns—which can require millions of spatial unknowns—but often only require a few dozen to a few hundred angular directions. Second, there are highly optimized, matrix-free transport solver methods—so called transport sweeps (cf. [24, 26, 27, 32])—that allow very efficient solutions of the SN equations (note that implicit time-stepping schemes are needed for TRT, due to its stiffness). In particular, SN methods do not require explicitly forming sparse matrices. In contrast, a standard DLR scheme would involve forming and solving the solution of an $r_0 N_x \times r_0 N_x$ non-symmetric sparse system. This makes it challenging to out-perform SN methods in both memory and computational cost.

Inspired by the recent collocation-based DLR method in (cf. [10, 9], [16], [25], and [33]), we develop an SN-like DLR method. The scheme resembles a traditional SN method, but with angular discretization points $\Omega^{(i)}(t)$, $i = 1, \dots, r_0$, that are dynamically selected in time from the (evolving) DLR angular basis functions $W_i(\Omega, t)$. This allows us to use the highly optimized transport sweep solvers from a traditional SN method as our primary computational kernel. In addition, we show in both theory and practice that the traditional diffusion-synthetic acceleration method (DSA) for preconditioning in the so-called diffusion limit works without modification. As a result, we are able to use the compression features of DLR in SN production codes with little modification, and with essentially no additional computational overhead. We note that a sweep-like method is developed in [30], but involves inverting $2^{\text{dim}} r_0 \times 2^{\text{dim}} r_0$ matrices for each spatial mesh element during the sweep and is limited to structured meshes; in contrast, our approach involves inverting only $2^{\text{dim}} \times 2^{\text{dim}}$ matrices in each spatial element for each of the r_0 directions, and can use state-of-the-art transport sweeps for this purpose.

We also present an alternative, more traditional DLR method for TRT that achieves efficiency in a different way. As a classic DLR method, it is based on Galerkin projection of the TRT equations on to angular and spatial basis functions at the beginning of each time step. This results in a PN-like DLR method, although in contrast to the standard PN method—which employs spherical harmonics as angular basis functions—the angular basis functions in the PN-like DLR scheme evolve in time to (nearly) minimize the solution residual for a fixed rank. Sweep solvers, which are SN-specific, are unavailable to PN methods, and while there have been advances in applying multigrid solvers to hyperbolic problems such as transport [17, 8, 7], such approaches are not yet competitive with sweep-based SN methods. However, in combination with DLR compression, this PN-like DLR method attains efficiency through an even-parity reformulation that transforms the first-order transport system into a pair of second-order problems. This results in two positive-definite $r_0 N_x \times r_0 N_x$ sparse matrix inversions for each time step, for which efficient algebraic multigrid solvers can be used for their solutions. In addition, the even-parity formulation avoids the need for diffusion acceleration or iterations on a given time step, as long as we ensure that the constant basis function in angle is contained within our DLR angular basis.

Section 2 presents the TRT equations and their reduction to a linear transport problem with effective scattering via Newton linearization. Our PN-like and SN-like DLR methods are presented in Sections 3-4. Finally, Section 5 demonstrates these DLR methods on several challenging test problems. The numerical experiments show that the SN-like DLR method can give improved accuracy for the same computational cost as a gold-standard SN method on a challenging benchmark problem [4].

2. Numerical formulation of thermal radiative transfer (TRT)

We begin by describing the basic TRT system of equations. The system describes the coupling between radiation energy density ($\psi(\mathbf{x}, \Omega, t)$) and material temperature (T). T is lower dimensional and is not factorized by DLR, so we also discuss the linearized time stepping approach for the temperature equation that is used throughout by both standard SN and DLR methods. The DLR factorization applies to $\psi(\mathbf{x}, \Omega, t)$, so we leave the description of discretization of the radiation energy density equation within each DLR method to their respective sections.

2.1. TRT equations

The frequency-averaged (i.e., grey) TRT equations for the material temperature $T(\mathbf{x}, t)$ and the photon energy distribution function $\psi(\mathbf{x}, \Omega, t)$ are given by [5]

$$\frac{1}{c} \frac{\partial \psi}{\partial t} + \Omega \cdot \nabla_{\mathbf{x}} \psi + \sigma(T) \psi = \sigma(T) B(T), \quad \mathbf{x} \in \mathcal{X}, \quad (1)$$

$$\psi(\mathbf{x}, \Omega, t) = 0, \quad \Omega \cdot \mathbf{n}(\mathbf{x}) \leq 0, \quad \mathbf{x} \in \partial \mathcal{X}, \quad (2)$$

$$\rho c_v(T) \frac{\partial T}{\partial t} = \sigma(T) (\varphi - 4\pi B(T)). \quad (3)$$

Here ρ denotes the material density, $c_v(T)$ denotes the temperature-dependent specific heat, $\sigma(T)$ denotes the temperature-dependent absorption opacity, φ denotes the angularly averaged intensity,

$$\varphi(\mathbf{x}) = \int_{\mathbb{S}^2} \psi(\mathbf{x}, \Omega) d\Omega.$$

For simplicity, we only consider vacuum boundary conditions (2) in this paper; however, the presented DLR methods extend trivially to more general boundary conditions.

2.2. Backward Euler discretization of the temperature equation and its linearization

We discretize equation (3) as follows

$$\rho c_v(T_0) (T - T_0) = \Delta t \sigma(T_0) (\varphi - 4\pi B(T)). \quad (4)$$

As is standard, we treat the temperature dependence of the opacity and specific heat explicitly, and treat the stiff emission term $B(T)$ implicitly.

As is standard, we obtain an approximation of the new temperature T in equation (4) via a Newton linearization [1] about the current temperature T_0 . This linearization yields a local $\mathcal{O}(\Delta t^2)$ time-stepping error, and results in an overall time-stepping scheme—for both DLR and standard SN methods—that in practice is as stable as the fully implicit backward Euler scheme.

In particular, a standard calculation yields the linear transport equation with pseudo-scattering over the time step $t \in [t_0, t_0 + \Delta t]$,

$$\frac{1}{c} \frac{\partial \psi}{\partial t} + \Omega \cdot \nabla_{\mathbf{x}} \psi + \sigma \psi = \frac{1}{4\pi} \sigma_s(T_0) \varphi + q(T_0), \quad (5)$$

where the pseudo-scattering opacity $\sigma_s(T_0)$ and the source term $q(T_0)$ are defined as

$$\sigma_s(T_0) = \left(\frac{4\pi \Delta t \sigma(T_0) \frac{\partial B}{\partial T}(T_0)}{\rho c_v(T_0) + 4\pi \Delta t \sigma(T_0) \frac{\partial B}{\partial T}(T_0)} \right) \sigma(T_0), \quad (6)$$

$$q(T_0) = \sigma(T_0) B(T_0) - \sigma \frac{\partial B}{\partial T}(T_0) \frac{4\pi \Delta t \sigma(T_0) B(T_0) + \rho c_v(T_0) T_0}{\rho c_v + 4\pi \sigma(T_0) \Delta t \frac{\partial B}{\partial T}(T_0)}. \quad (7)$$

Once we solve for ψ , we can update our approximation to temperature at the next time step,

$$T \approx T_0 + \frac{\Delta t \sigma(T_0) (\varphi - 4\pi B(T_0)) - \rho c_v(T_0) T_0}{\rho c_v(T_0) + 4\pi \Delta t \sigma(T_0) \frac{\partial B}{\partial T}(T_0)}. \quad (8)$$

3. A PN-like DLR scheme using an even-parity formulation of transport

Here we develop a classical DLR based TRT scheme, with the twist that we employ an even-parity transformation that allows the system to be solved efficiently using algebraic multigrid solvers. The result is a PN-like DLR formulation that is efficiently solvable and exhibits no ray effects

We approximate the solution using a time-evolving SVD-like low-rank representation

$$\psi(\mathbf{x}, \Omega, t) = \sum_{i,j=1}^{r_0} X_i(\mathbf{x}, t) S_{ij}(t) W_j(\Omega, t) = \mathbf{W}^T(\Omega, t) \mathbf{S}(t)^T \mathbf{X}(\mathbf{x}, t), \quad (9)$$

where

$$\mathbf{X}(\mathbf{x}, t) = \begin{pmatrix} X_1(\mathbf{x}, t) \\ \vdots \\ X_{r_0}(\mathbf{x}, t) \end{pmatrix}, \quad \mathbf{W}(\boldsymbol{\Omega}, t) = \begin{pmatrix} W_1(\boldsymbol{\Omega}, t) \\ \vdots \\ W_{r_0}(\boldsymbol{\Omega}, t) \end{pmatrix}.$$

Here the functions X_i , $i = 1, \dots, r_0$, are orthonormal,

$$\langle X_i(\cdot, t), X_j(\cdot, t) \rangle_{\mathcal{X}} = \int_{\mathcal{X}} X_i(\mathbf{x}, t) X_j(\mathbf{x}, t) d\mathbf{x} = \delta_{i,j}. \quad (10)$$

Similarly, the functions W_j are orthonormal,

$$\langle W_i(\cdot, t), W_j(\cdot, t) \rangle_{\mathcal{X}} = \int_{\mathbb{S}^2} W_i(\boldsymbol{\Omega}, t) W_j(\boldsymbol{\Omega}, t) d\boldsymbol{\Omega} = \delta_{i,j}. \quad (11)$$

We frequently express the low-rank representation (9) in the equivalent forms

$$\begin{aligned} \psi(\mathbf{x}, \boldsymbol{\Omega}, t) &= \sum_{i,j=1}^{r_0} X_i(\mathbf{x}, t) S_{ij}(t) W_j(\boldsymbol{\Omega}, t) \\ &= \sum_{j=1}^{r_0} K_j(\mathbf{x}, t) W_j(\boldsymbol{\Omega}, t) \end{aligned} \quad (12)$$

$$= \sum_{i=1}^{r_0} X_i(\mathbf{x}, t) L_i(\boldsymbol{\Omega}, t), \quad (13)$$

where

$$K_j(\mathbf{x}, t) = \sum_{i=1}^{r_0} X_i(\mathbf{x}, t) S_{ij}(t), \quad L_i(\boldsymbol{\Omega}, t) = \sum_{j=1}^{r_0} S_{ij}(t) W_j(\boldsymbol{\Omega}, t). \quad (14)$$

Write the transport equation (5) in the abstract form

$$\frac{\partial \psi}{\partial t} = \mathcal{L}\psi + q. \quad (15)$$

Differentiating equations (12) and (13) with respect to time t and using the orthogonality constraints (10)-(11), it is straightforward to show (see Appendix 7.1) that

$$\dot{L}_j = \left\langle \frac{\partial \psi}{\partial t}, X_j \right\rangle_{\mathcal{X}}, \quad \dot{K}_j = \left\langle \frac{\partial \psi}{\partial t}, W_j \right\rangle_{\mathbb{S}^2}, \quad \dot{S}_{ij} = \left\langle \frac{\partial \psi}{\partial t}, X_i W_j \right\rangle_{\mathcal{X} \times \mathbb{S}^2}, \quad (16)$$

and

$$\frac{\partial \psi}{\partial t} = \sum_{j=1}^{r_0} \dot{K}_j W_j + \sum_{i=1}^{r_0} \dot{L}_i X_i - \sum_{i,j=1}^{r_0} X_i \dot{S}_{ij} W_j. \quad (17)$$

Combining equations (15) and (16),

$$\dot{L}_j = \sum_{i=1}^{r_0} \left\langle \mathcal{L}(X_i L_i) + q, X_j \right\rangle_{\mathcal{X}}, \quad (18)$$

$$\dot{K}_j = \sum_{i=1}^{r_0} \left\langle \mathcal{L}(K_i W_i) + q, W_j \right\rangle_{\mathbb{S}^2}. \quad (19)$$

$$\dot{S}_{ij} = \sum_{i',j'=1}^{r_0} S_{i'j'} \langle \mathcal{L}(X_{i'}W_{j'}) + q, X_i W_j \rangle_{\mathcal{X} \times \mathbb{S}^2}, \quad (20)$$

We discretize equations (18)-(20) in time via backward Euler and lag the DLR basis functions in time X_j and W_j . In particular, define $X_{0,i}(\mathbf{x}) = X_i(\mathbf{x}, t_0)$ and $W_{0,j}(\boldsymbol{\Omega}) = W_j(\boldsymbol{\Omega}, t_0)$. Then

$$\frac{L_j - L_{0,j}}{\Delta t} = \sum_{i=1}^{r_0} \langle \mathcal{L}(X_{0,i}L_i) + q, X_{0,j} \rangle_{\mathcal{X}}, \quad (21)$$

$$\frac{K_j - K_{0,j}}{\Delta t} = \sum_{i=1}^{r_0} \langle \mathcal{L}(W_{0,i}K_i) + q, W_{0,j} \rangle_{\mathbb{S}^2}, \quad (22)$$

$$\frac{S_{ij} - S_{0,ij}}{\Delta t} = \sum_{i',j'=1}^{r_0} S_{i'j'} \langle \mathcal{L}(X_{0,i'}W_{0,j'}) + q, X_{0,i}W_{0,j} \rangle_{\mathcal{X} \times \mathbb{S}^2}. \quad (23)$$

We supplement the above equations with equation (4) for the updated temperature T .

Once we solve the equations (4) and (21)-(23) for T , K_j , L_j , and S_{ij} at the next time $t = t_0 + \Delta t$, we then compute the updated solution via equation (17),

$$\begin{aligned} \psi &= \psi_0 + \Delta t \frac{\partial \psi}{\partial t} \\ &= \psi_0 + \sum_{j=1}^{r_0} (K_j - K_{0,j}) W_j + \sum_{i=1}^{r_0} (L_i - L_{0,i}) X_i - \sum_{i,j=1}^{r_0} X_i (S_{ij} - S_{0,ij}) W_j. \end{aligned} \quad (24)$$

The representation (24) for ψ at the next time step increases the rank from r_0 to $2r_0$; we perform a truncated SVD to reduce the representation back down to rank r_0 . In more detail,

$$\psi(\mathbf{x}, \boldsymbol{\Omega}) = \mathbf{Y}(\mathbf{x})^T \mathbf{Z}(\boldsymbol{\Omega}),$$

where, e.g.,

$$Y_j = \begin{cases} (K_j - K_{0,j}) - \sum_{i=1}^{r_0} X_i (S_{ij} - S_{0,ij}), & 1 \leq j \leq r_0, \\ X_i, & r_0 + 1 \leq j \leq 2r_0. \end{cases}$$

We can orthogonalize the basis functions $Y_j(\mathbf{x})$ via stabilized Gram Schmidt, $\mathbf{Y}(\mathbf{x}) = R_Y \mathbf{U}(\mathbf{x})$. Similarly, $\mathbf{Z}(\boldsymbol{\Omega}) = R_Z \mathbf{V}(\boldsymbol{\Omega})$. Then

$$\psi(\mathbf{x}, \boldsymbol{\Omega}) = \mathbf{Y}(\mathbf{x})^T \mathbf{Z}(\boldsymbol{\Omega}) = \mathbf{U}(\mathbf{x})^T (R_Y^T R_Z) \mathbf{V}(\boldsymbol{\Omega}).$$

We then employ a truncated SVD on the $2r_0 \times 2r_0$ matrix $R_Y^T R_Z$ to round back down to a rank r approximation for $\psi(\mathbf{x}, \boldsymbol{\Omega})$.

We now discuss the solution of equations (21)-(23) in more detail in Sections 3.1-3.4.

3.1. Even parity formulation of transport for the K step

Fast transport sweeps are unavailable to PN formulations, and multigrid solvers do not yet give competitive efficiency when inverting the matrices that come from direct discretization of equation (5). To deal with this, we use the even parity approach from transport to reformulate the first-order system into a pair of second-order systems (cf. [23]) that are amenable to fast algebraic multigrid solvers. This trades one slow solve for two fast ones, and in

combination with DLR compression gives an efficient solver. Here we briefly describe the even parity formulation for standard transport and then adapt its use to DLR in the next section.

Consider the backward Euler discretization of the steady-state equation (5),

$$\boldsymbol{\Omega} \cdot \nabla_{\mathbf{x}} \psi + \sigma_t \psi - \frac{1}{4\pi} \sigma_s \varphi = Q. \quad (25)$$

First we decompose the solution into even and odd components in angle,

$$\psi_{\pm}(\mathbf{x}, \boldsymbol{\Omega}) = \frac{1}{2} (\psi(\mathbf{x}, \boldsymbol{\Omega}) \pm \psi(\mathbf{x}, -\boldsymbol{\Omega})).$$

Then it can be shown (cf. [23]) that ψ_- satisfies

$$-\boldsymbol{\Omega} \cdot \nabla_{\mathbf{x}} \left(\frac{1}{\sigma_t} \boldsymbol{\Omega} \cdot \nabla \psi_- \right) + \sigma_t \psi_- = Q_- - \boldsymbol{\Omega} \cdot \nabla_{\mathbf{x}} \left(\frac{1}{\sigma_t} Q_+ \right), \quad \mathbf{x} \in \mathcal{X}, \quad (26)$$

$$|\mathbf{n} \cdot \boldsymbol{\Omega}| \psi_- + \mathbf{n} \cdot \boldsymbol{\Omega} \left(\frac{1}{\sigma_t} \boldsymbol{\Omega} \cdot \nabla_{\mathbf{x}} \psi_- \right) = \mathbf{n} \cdot \boldsymbol{\Omega} \frac{1}{\sigma_t} Q_+, \quad \mathbf{x} \in \partial \mathcal{X}. \quad (27)$$

Similarly,

$$-\boldsymbol{\Omega} \cdot \nabla_{\mathbf{x}} \left(\frac{1}{\sigma_t} \boldsymbol{\Omega} \cdot \nabla_{\mathbf{x}} \psi_+ \right) + \sigma_t \psi_+ - \frac{\sigma_s}{4\pi} \varphi_+ = Q_+ - \boldsymbol{\Omega} \cdot \nabla_{\mathbf{x}} \left(\frac{1}{\sigma_t} Q_- \right), \quad \mathbf{x} \in \mathcal{X}, \quad (28)$$

$$|\mathbf{n} \cdot \boldsymbol{\Omega}| \psi_+ + \mathbf{n} \cdot \boldsymbol{\Omega} \left(\frac{1}{\sigma_t} \boldsymbol{\Omega} \cdot \nabla_{\mathbf{x}} \psi_+ \right) = \mathbf{n} \cdot \boldsymbol{\Omega} \frac{1}{\sigma_t} Q_-, \quad \mathbf{x} \in \partial \mathcal{X}. \quad (29)$$

3.2. K step for PN-like DLR method

We now explicitly compute the matrix system for equations (22), starting from the even-parity formulation detailed in Section 3.1.

Importantly, we always enforce that $W_{0,0}(\boldsymbol{\Omega}) = 1/\sqrt{4\pi}$. This ensures that Galerkin projection for the K step can be solved efficiently without iteration. We also use even and odd constructions of the angular basis functions,

$$W_{0,j}^+(\boldsymbol{\Omega}) = \frac{W_{0,j}(\boldsymbol{\Omega}) + W_{0,j}(-\boldsymbol{\Omega})}{2}, \quad W_{0,j}^-(\boldsymbol{\Omega}) = \frac{W_{0,j}(\boldsymbol{\Omega}) - W_{0,j}(-\boldsymbol{\Omega})}{2}, \quad (30)$$

when we construct the K step equations.

To do so, suppose that

$$\psi_{\pm}(\mathbf{x}, \boldsymbol{\Omega}) = \sum_{j=1}^{r_0} W_{0,j}^{\pm}(\boldsymbol{\Omega}) K_j^{\pm}(\mathbf{x}).$$

Define

$$A_{j,j'}^{\pm} = \left\langle \boldsymbol{\Omega} \boldsymbol{\Omega}^T W_{0,j}^{\pm}, W_{0,j'}^{\pm} \right\rangle_{\mathbb{S}^2}, \quad \kappa_{j,j'} = \left\langle \boldsymbol{\Omega} W_{0,j}^{\pm}, W_{0,j'}^{\pm} \right\rangle_{\mathbb{S}^2}, \quad \beta_{j,j'}(\mathbf{x}) = \left\langle |\mathbf{n}(\mathbf{x}) \cdot \boldsymbol{\Omega}| W_{0,j}^{\pm}, W_{0,j'}^{\pm} \right\rangle_{\mathbb{S}^2}.$$

Then projecting equations (28) and (29) on to the angular basis functions $W_{0,j}^{\pm}(\boldsymbol{\Omega})$, a direct calculation shows that, $j = 1, \dots, r_0$,

$$-\sum_{j=1}^{r_0} A_{j,j'}^+ \nabla_{\mathbf{x}} \left(\frac{1}{\sigma_t} \nabla_{\mathbf{x}} K_j^+ \right) + \sigma_t K_{j'}^+ + \delta_{j',0} \sqrt{\frac{1}{4\pi}} \sigma_s K_0^+ = Q_{j'}^+ - \sum_{j=1}^{r_0} \nabla_{\mathbf{x}} \cdot \left(\frac{1}{\sigma_t} Q_j^- \kappa_{j,j'}^+ \right), \quad \mathbf{x} \in \mathcal{X}, \quad (31)$$

with boundary conditions

$$\sum_{j=1}^{r_0} \beta_{j,j'}^+ K_j^+ + \sum_{j=1}^{r_0} \mathbf{n} \cdot \frac{1}{\sigma_t} \left(A_{j,j'}^+ \nabla_{\mathbf{x}} K_j^+ \right) = \sum_{j=1}^{r_0} \mathbf{n} \cdot \frac{1}{\sigma_t} \left(\kappa_{j,j'}^+ Q_j^- \right), \quad \mathbf{x} \in \partial \mathcal{X}. \quad (32)$$

An analogous system holds for K_j^- , $j = 1, \dots, r$:

$$- \sum_{j=1}^{r_0} A_{j,j'}^- \nabla_{\mathbf{x}} \left(\frac{1}{\sigma_t} \nabla_{\mathbf{x}} K_j^- \right) + \sigma_t K_j^- = Q_{j'}^- - \sum_{j=1}^{r_0} \nabla_{\mathbf{x}} \cdot \left(\frac{1}{\sigma_t} Q_{j'}^+ \kappa_{j,j'}^- \right), \quad \mathbf{x} \in \mathcal{X}, \quad (33)$$

with boundary conditions

$$\sum_{j=1}^{r_0} \beta_{j,j'}^- K_j^- + \sum_{j=1}^{r_0} \mathbf{n} \cdot \frac{1}{\sigma_t} \left(A_{j,j'}^- \nabla_{\mathbf{x}} K_j^- \right) = \sum_{j=1}^{r_0} \mathbf{n} \cdot \frac{1}{\sigma_t} \left(\kappa_{j,j'}^- Q_j^+ \right), \quad \mathbf{x} \in \partial \mathcal{X}. \quad (34)$$

Note that the equations (33)-(34) are positive-definite and their space-discretized version are efficiently solved with algebraic multigrid methods.

3.3. L step for PN-like DLR method

Define

$$B_{i,j}(\Omega) = \langle \nabla_{\mathbf{x}} X_{0,j}, X_{0,i} \rangle_{\mathcal{X}} \cdot \Omega + \sum_j \langle \sigma_t X_{0,j}, X_{0,i} \rangle_{\mathcal{X}},$$

$$(M_s)_{i,j} = \langle \sigma_s X_{0,j}, X_{0,i} \rangle_{\mathcal{X}}.$$

Then projecting equation (25) on to the r_0 spatial basis functions $X_{0,j}(\mathbf{x})$, a straight-forward calculation shows that

$$\sum_{j=1}^{r_0} B_{i,j}(\Omega) L_j(\Omega) - \frac{1}{4\pi} \sum_{j=1}^{r_0} (M_s)_{i,j} \int_{\mathbb{S}^2} L_j d\Omega' = q_{0,i}(\Omega). \quad (35)$$

To efficiently solve the L system (35), define

$$\mathbf{L}(\Omega) = \begin{pmatrix} L_1(\Omega) \\ \vdots \\ L_r(\Omega) \end{pmatrix}, \quad \mathbf{q}(\Omega) = \begin{pmatrix} q_{0,1}(\Omega) \\ \vdots \\ q_{0,r}(\Omega) \end{pmatrix}, \quad \bar{\mathbf{L}} = \begin{pmatrix} \int_{\mathbb{S}^2} L_1(\Omega') d\Omega' \\ \vdots \\ \int_{\mathbb{S}^2} L_r(\Omega') d\Omega' \end{pmatrix}.$$

Then

$$B(\Omega) L(\Omega) - \frac{1}{4\pi} M_s \bar{\mathbf{L}} = \mathbf{q}(\Omega). \quad (36)$$

Define

$$\bar{C} = \int_{\mathbb{S}^2} (B(\Omega))^{-1} d\Omega, \quad \bar{\zeta} = \int_{\mathbb{S}^2} B(\Omega')^{-1} \mathbf{q}(\Omega') d\Omega'.$$

Then

$$\bar{\mathbf{L}} - \bar{C} \frac{1}{4\pi} M_s \bar{\mathbf{L}} = \bar{\zeta}.$$

Once we solve for $\bar{\mathbf{L}}$, we solve equation (36) for each angle Ω independently.

3.4. S step for PN-like DLR method

Define

$$\mathbf{b}_{i,i'} = \langle \nabla_{\mathbf{x}} X_{0,i}, X_{0,i'} \rangle_{\mathcal{X}}, \quad \boldsymbol{\kappa}_{j,j'} = \langle \Omega W_{0,j}, W_{0,j'} \rangle_{\mathbb{S}^2}.$$

Then projecting equation (25) on to the r_0^2 basis functions $X_{0,i}(\mathbf{x}) W_{0,j}(\Omega)$,

$$\sum_{i,j=1}^{r_0} S_{ij} \mathbf{b}_{i,i'} \boldsymbol{\kappa}_{j,j'} + \sum_{i,j} (M_t)_{i,i'} S_{ij} \delta_{j,j'} - \sum_{i,j=1}^{r_0} \frac{1}{4\pi} S_{ij} (M_s)_{i,i'} \overline{W}_{j'} \overline{W}_j = q_{i',j'}.$$

Here

$$q_{i',j'} = S_{0,i',j'} + \langle q, X_{0,i'} W_{0,j'} \rangle_{\mathcal{X} \times \mathbb{S}^2}.$$

4. An SN-like DLR scheme

We present an SN-like DLR method for solving the TRT equations. The key advantage of this scheme is that we can leverage highly efficient sweep-based methods

We note that the sweep-based method in [30] requires the inversion of $r_0 2^{\text{dim}} \times r_0 2^{\text{dim}}$ matrices in each mesh element; our collocation-based scheme instead requires the inversion of matrices of size $2^{\text{dim}} \times 2^{\text{dim}}$ in each mesh element for rank r_0 worth of angles. In practice, this makes this version of the sweeping scheme competitive with SN methods even for small SN orders. In addition, our collocation-based scheme mitigates, but does not eliminate ray effects, as demonstrated by the hohlraum numerical experiments in Section 5.2; in such cases, there can be major advantages to the scheme in [30], as well as the PN-like DLR method presented in this section.

4.1. Computing the scalar flux from collocation angles

Suppose that we have approximations to $\psi(\mathbf{x}, \Omega_i(t), t)$ at specific angles $\Omega^{(i)}(t)$, $i = 1, \dots, r_0$. We want to approximate $\psi(\mathbf{x}, \Omega, t)$ in terms of the orthonormal angular functions $W_j(\Omega, t)$,

$$\psi(\mathbf{x}, \Omega, t) \approx \sum_{j=1}^{r_0} K_j(\mathbf{x}, t) W_j(\Omega, t). \quad (37)$$

To do so, we solve the linear system

$$\psi(\mathbf{x}, \Omega^{(i)}(t), t) = \sum_{j=1}^{r_0} K_j(\mathbf{x}, t) W_j(\Omega^{(i)}(t), t), \quad i = 1, \dots, r_0.$$

Define $\hat{W}_{ij}(t) = W_j(\Omega^{(i)}(t), t)$, and

$$\mathbf{K}(\mathbf{x}, t) = \begin{pmatrix} K_1(\mathbf{x}, t) \\ \vdots \\ K_{r_0}(\mathbf{x}, t) \end{pmatrix}, \quad \mathbf{\Psi}(\mathbf{x}, t) = \begin{pmatrix} \psi(\mathbf{x}, \Omega^{(1)}(t), t) \\ \vdots \\ \psi(\mathbf{x}, \Omega^{(r_0)}(t), t) \end{pmatrix}.$$

Then

$$\mathbf{\Psi}(\mathbf{x}, t) = \hat{W}(t) \mathbf{K}(\mathbf{x}, t).$$

It follows that we can reconstruct

$$\mathbf{K}(\mathbf{x}, t) = \hat{W}(t)^{-1} \mathbf{\Psi}(\mathbf{x}, t).$$

From equation (37), we also have that

$$\int_{\mathbb{S}^2} \psi(\mathbf{x}, \Omega, t) d\Omega \approx \sum_{j=1}^{r_0} K_j(\mathbf{x}, t) \int_{\mathbb{S}^2} W_j(\Omega, t) d\Omega$$

$$= \beta^T (\hat{W}^{-1} \Psi(\mathbf{x}, t)),$$

where

$$\beta_j = \int_{\mathbb{S}^2} W_j(\Omega) d\Omega, \quad j = 1, \dots, r_0.$$

4.2. Discrete Empirical Interpolation Method (DEIM)

The DEIM algorithm proceeds iteratively in a manner entirely analogous to Gram-Schmidt orthogonalization. On the first step, we choose the first interpolation point $\Omega_1 \in \mathbb{S}^2$ that maximizes $|W_1(\Omega)|$,

$$\Omega_1 = \operatorname{argmax}_{\Omega} |W_1(\Omega)|.$$

Now, suppose at the $(j-1)$ st step we have constructed interpolation points $\Omega_1, \dots, \Omega_{j-1}$. Define the interpolatory projection

$$(P^{(j-1)} W_j)(\Omega) = \sum_{k=1}^{j-1} c_k^{(j-1)} W_k(\Omega),$$

where the coefficients $c_i^{(j-1)}$ are uniquely chosen to enforce the interpolation property

$$W_j(\Omega^{(i)}) = \sum_{k=1}^{j-1} c_k^{(j-1)} W_k(\Omega^{(i)}), \quad i = 1, \dots, j-1.$$

To find the next interpolation point $\Omega^{(j)}$, we subtract from W_j its interpolatory projection on to the previous $j-1$ basis functions W_1, \dots, W_{j-1} :

$$R_j(\Omega) = W_j(\Omega) - (P^{(j-1)} W_j)(\Omega).$$

Then we define the next interpolation point via

$$\Omega_j = \operatorname{argmax}_{\Omega} |R_j(\Omega)|.$$

Note that, by construction,

$$R_j(\Omega^{(i)}) = W_j(\Omega^{(i)}) - \sum_{i=1}^{j-1} c_i^{(j-1)} W_i(\Omega^{(i)}) = 0, \quad i = 1, \dots, j-1.$$

Therefore, $\Omega^{(j)} \notin \{\Omega^{(1)}, \dots, \Omega^{(j-1)}\}$.

4.3. Collocation-based Dynamic Low Rank (DLR) Method

The main algorithm starts with the initial representation

$$\psi^{(0)}(\mathbf{x}, \Omega) = \psi(\mathbf{x}, \Omega, t_0) = \mathbf{W}^T(\Omega, t_0) S(t_0)^T \mathbf{X}(\mathbf{x}, t_0).$$

We first select r_0 angles $\Omega^{(j)}(t_0)$, $j = 1, \dots, r_0$, using DEIM algorithm discussed in Section 4.2 applied to the angular basis functions $\mathbf{W}(\Omega, t_0)$ at the beginning of the time step. We then evaluate the initial condition for the next time step at these new angles,

$$\begin{aligned} \psi_j^{(0)}(\mathbf{x}) &= \psi(\mathbf{x}, \Omega^{(j)}(t_0), t_0) \\ &= \sum_{k=1}^{r_0} L_k(\Omega^{(j)}(t_0), t_0) X_k(\mathbf{x}, t_0). \end{aligned}$$

Next, define

$$\psi_j(\mathbf{x}, t) = \psi(\mathbf{x}, \Omega^{(j)}(t_0), t), \quad \Psi(\mathbf{x}, t) = \begin{pmatrix} \psi(\mathbf{x}, \Omega^{(1)}(t_0), t) \\ \vdots \\ \psi(\mathbf{x}, \Omega^{(r_0)}(t_0), t) \end{pmatrix}.$$

Then we solve the following equations (“column constraints”) for Ψ ,

$$\Omega^{(j)} \cdot \nabla_{\mathbf{x}} \psi_j + \left(\sigma + \frac{1}{c\Delta t} \right) \psi_j = \frac{1}{4\pi} \sigma_s \beta^T (\hat{W}^{-1} \Psi) + q + \frac{1}{c\Delta t} \psi_j^{(0)}, \quad (38)$$

where we use the relationship derived in Section 4.1,

$$\int_{\mathbb{S}^2} \psi(\mathbf{x}, \Omega, t) d\Omega \approx \beta^T (\hat{W}^{-1} \Psi(\mathbf{x}, t)).$$

In non-DLR production transport codes, the analog of equation (38) is generally solved with “source iteration”, a type of fixed point iteration where the left hand side operator is inverted each iteration using fast sweep algorithms while the entire right hand side is kept fixed for the inversion within an iteration but updated between them. The sweep algorithms depend on angular information being uncoupled and traveling along discrete angles on the left hand side, allowing the flow of dependencies to be traced in space from the problem boundaries along each fixed direction, giving a fast triangular solve for each angle. This same structure holds in (38), allowing standard sweep and source iteration implementations to be carried over to the SN-like DLR method with minimal conversion.

Source iteration with sweeps along discrete angles has the physical interpretation of each iteration tracing light between scattering events, with scattering occurring when the right hand side is updated between iterations. Therefore, in highly scattering media, the number of iterations (scatter events) will be high before the final global distribution of light (for the time step) is fully converged Diffusion synthetic acceleration, described in Section 4.5, is used to accelerate convergence in the face of this.

After solving equation (38), we orthonormalize $\Psi(\mathbf{x})$ via stabilized Gram-Schmidt,

$$\Psi(\mathbf{x}, t) = R(t) \mathbf{X}(\mathbf{x}, t),$$

where

$$\int_{\mathcal{X}} X_i(\mathbf{x}) X_j(\mathbf{x}) d\mathbf{x} = \delta_{i,j}.$$

For “row constraints”, we project equation (5) using the new spatial basis functions,

$$\Omega \cdot \langle \nabla_{\mathbf{x}} \psi, X_i \rangle_{\mathcal{X}} + \left\langle \left(\sigma + \frac{1}{c\Delta t} \right) \psi, X_i \right\rangle_{\mathcal{X}} = \frac{1}{4\pi} \langle \sigma_s \varphi, X_i \rangle_{\mathcal{X}} + \left\langle q + \frac{1}{c\Delta t} \psi^{(0)}, X_i \right\rangle_{\mathcal{X}}. \quad (39)$$

If we make the Galerkin approximation

$$\psi(\mathbf{x}, \Omega, t) = \sum_{j=1}^{r_0} L_j(\Omega, t) X_j(\mathbf{x}, t),$$

then we have the equations for $L_j(\Omega, t)$,

$$(A + M_t) \mathbf{L} = \frac{1}{4\pi} M_s \int_{\mathbb{S}^2} \mathbf{L} d\Omega + \mathbf{Q}, \quad (40)$$

where

$$\mathbf{L}(\Omega, t) = \begin{pmatrix} L_1(\Omega, t) \\ \vdots \\ L_{r_0}(\Omega, t) \end{pmatrix},$$

$$A_{i,j} = \sum_k \Omega_k \left\langle \frac{\partial X_j}{\partial x_k}, X_i \right\rangle_{\mathcal{X}}, \quad (M_t)_{i,j} = \left\langle \left(\sigma + \frac{1}{c\Delta t} \right) X_j, X_i \right\rangle_{\mathcal{X}},$$

and

$$(M_s)_{i,j} = \left\langle \sigma_s X_j, X_i \right\rangle_{\mathcal{X}}, \quad Q_i = \left\langle q + \frac{1}{c\Delta t} \psi^{(0)}, X_i \right\rangle_{\mathcal{X}}.$$

Note that we can compute $Q_i(\Omega, t)$ using the low-rank factorization of $\psi(\mathbf{x}, \Omega, t_0)$:

$$\begin{aligned} Q_i(\Omega, t) &= \left\langle q(\cdot, t) + \frac{1}{c\Delta t} \psi(\cdot, \Omega, t_0), X_i(\cdot, t) \right\rangle_{\mathcal{X}} \\ &= \langle q(\cdot, t), X_i(\cdot, t) \rangle_{\mathcal{X}} + \frac{1}{c\Delta t} \sum_{j=1}^{r_0} L_i(\Omega, t_0) \langle X_i(\cdot, t_0), X_i(\cdot, t) \rangle_{\mathcal{X}}. \end{aligned}$$

Next, orthonormalize the L_j functions,

$$L_j(\Omega, t) = \sum_{k=1}^{r_0} S_{jk}(t) W_k(\Omega, t) = (S(t) \mathbf{W}(t))_j(\Omega, t),$$

where

$$\int_{\mathbb{S}^2} W_i(\Omega) W_j(\Omega) d\Omega = \delta_{i,j}.$$

Then we finally obtain that

$$\begin{aligned} \psi(\mathbf{x}, \Omega, t) &= \mathbf{L}^T(\Omega, t) \mathbf{X}(\mathbf{x}, t) \\ &= \mathbf{W}^T(\Omega, t) S(t)^T \mathbf{X}(\mathbf{x}, t). \end{aligned}$$

We summarize the DLR solve in Algorithm 1. The input to this algorithm is initial condition,

$$\psi^{(0)}(\mathbf{x}, \Omega) = \sum_{k=1}^{r_0} L_k^{(0)}(\Omega) X_k^{(0)}(\mathbf{x}).$$

In addition,

$$L_j^{(0)}(\Omega) = \sum_{k=1}^{r_0} S_{jk}^{(0)} W_k^{(0)}(\Omega) = (S^{(0)} \mathbf{W}^{(0)})_j(\Omega),$$

where

$$\int_{\mathbb{S}^2} W_i^{(0)}(\Omega) W_j^{(0)}(\Omega) d\Omega = \delta_{i,j}.$$

4.4. Spatial discretization for collocation solve

In preparation for defining the DSA algorithm in the next section to accelerate the solve for (38), we here detail the spacial discretization of the equations, as it is imperative that DSA be derived consistently with it (see [2]).

Define

$$\mathbf{v}^T G_j \mathbf{u} = - \sum_e \int_{\kappa_e} \frac{\partial v}{\partial x_j} u d\mathbf{x}, \quad j = 1, 2, 3. \quad (41)$$

Also, define the angle-dependent face matrix

$$\mathbf{v}^T F_d \mathbf{u} = - \sum_f \int_{\Gamma_f} \mathbf{\Omega}^{(d)} \cdot \mathbf{n} [[v]] \{u\} dS + \frac{1}{2} \sum_f \int_{\Gamma_f} |\mathbf{\Omega}^{(d)} \cdot \mathbf{n}| [[u]] [[v]] dS.$$

Algorithm 1 SN-like DLR method for the time step update

1. Update the effective scattering and transport source using equations 6-7
2. Select r_0 angles $\Omega^{(j)}$, $j = 1, \dots, r_0$, using DEIM algorithm in Section 4.2 applied to $\mathbf{W}^{(0)}(\Omega)$.
3. Evaluate the initial condition at the new angles, for $j = 1, \dots, r_0$,

$$\psi_j^{(0)}(\mathbf{x}) = \psi^{(0)}(\mathbf{x}, \Omega^{(j)}) = \sum_{k=1}^{r_0} L_k^{(0)}(\Omega^{(j)}) X_k^{(0)}(\mathbf{x}).$$

4. Using fixed-point iteration, solve the SN-like system of r_0 equations

$$\Omega^{(j)} \cdot \nabla_{\mathbf{x}} \psi_j + \left(\sigma + \frac{1}{c\Delta t} \right) \psi_j = \frac{1}{4\pi} \sigma_s \beta^T (\hat{W}^{-1} \Psi) + q + \frac{1}{c\Delta t} \psi_j^{(0)},$$

where $\hat{W}_{ij} = W_j(\Omega^{(i)})$, $\beta_j = \int_{\mathbb{S}^2} W_j(\Omega) d\Omega$,

$$\psi_j(\mathbf{x}) = \psi(\mathbf{x}, \Omega^{(j)}), \quad \Psi(\mathbf{x}) = \begin{pmatrix} \psi_1(\mathbf{x}) \\ \vdots \\ \psi_{r_0}(\mathbf{x}) \end{pmatrix}.$$

Sweep algorithms are used to invert the left hand side operator each iteration. Applying DSA from Section 4.5 keeps the iteration count low.

5. Orthonormalize $\Psi(\mathbf{x})$ via stabilized Gram-Schmidt,

$$\Psi(\mathbf{x}) = R\mathbf{X}(\mathbf{x}), \quad \int_{\mathcal{X}} X_i(\mathbf{x}) X_j(\mathbf{x}) d\mathbf{x} = \delta_{i,j}.$$

6. Project the initial condition $\psi_j^{(0)}$ on to the r spatial basis functions X_j ,

$$\tilde{L}_j^{(0)} = \langle \psi^{(0)}, X_j \rangle_{\mathcal{X}} = \sum_{j=1}^{r_0} L_i^{(0)} \langle X_i^{(0)}, X_j \rangle_{\mathcal{X}}.$$

7. Solve

$$(A + M_t) \mathbf{L} = \frac{1}{4\pi} M_s \int_{\mathbb{S}^2} \mathbf{L} d\Omega + \mathbf{Q},$$

where

$$A_{i,j} = \sum_k \Omega_k \left\langle \frac{\partial X_j}{\partial x_k}, X_i \right\rangle_{\mathcal{X}}, \quad (M_t)_{i,j} = \left\langle \left(\sigma + \frac{1}{c\Delta t} \right) X_j, X_i \right\rangle_{\mathcal{X}},$$

$$(M_s)_{i,j} = \langle \sigma_s X_j, X_i \rangle_{\mathcal{X}}, \quad Q_i = \langle q, X_i \rangle_{\mathcal{X}} + \frac{1}{c\Delta t} \tilde{L}_i^{(0)}.$$

8. Orthonormalize the L_j functions, $j = 1, \dots, r$,

$$L_j(\Omega) = \sum_{k=1}^{r_0} S_{jk} W_k(\Omega) = (SW)_j(\Omega), \quad \int_{\mathbb{S}^2} W_i W_j d\Omega = \delta_{i,j}.$$

9. Update the material temperature using equation (8) and the new mean intensity φ

Finally, define the following mass matrices

$$\mathbf{v}^T \mathbf{M}_t \mathbf{u} = - \sum_e \int_{\kappa_e} \sigma_t u v d\mathbf{x},$$

$$\mathbf{v}^T \mathbf{M}_a \mathbf{u} = - \sum_e \int_{\kappa_e} \sigma_a u v d\mathbf{x},$$

$$\mathbf{v}^T \mathbf{M} \mathbf{u} = - \sum_e \int_{\kappa_e} u v d\mathbf{x}.$$

Then equation (38) is discretized by

$$(\Omega^{(d)} \cdot \mathbf{G} + F_d) \boldsymbol{\psi}_d + \left(M_a + \frac{1}{c\Delta t} M \right) \boldsymbol{\psi}_d = \frac{1}{4\pi} M_s \boldsymbol{\beta}^T (\hat{W}^{-1} \boldsymbol{\psi}) + \mathbf{q}_d + \frac{1}{c\Delta t} M \boldsymbol{\psi}_{0,d}.$$

Here

$$\boldsymbol{\psi} = \begin{pmatrix} \boldsymbol{\psi}_1 \\ \vdots \\ \boldsymbol{\psi}_{r_0} \end{pmatrix}.$$

4.5. Diffusion Synthetic Acceleration (DSA) for SN-like DLR method

It is well-understood that, for “optically thick” problems that are characterized by small photon mean free path relative to the mesh resolution, a basic fixed-point iteration to solve spatially discretized version of equation (5) converges arbitrarily slowly (in fact, like the inverse square of the photon mean free path). Diffusion Synthetic Acceleration (DSA) (cf. [20], [22], and [21]) is the traditional means to restore fast convergence; see [2] for an excellent discussion of iterative methods for solving linear transport equations such as (5), and how DSA gives convergence independent of the photon mean free path.

The need for DSA acceleration carries over to the equation (38). It is crucial for iterative efficiency (see [2]) that a so-called consistent DSA method is derived. We briefly outline how DSA can be used, with little modification, to efficiently accelerate the fixed-point solution to equation (38); a detailed derivation is included in Section 7.2 of the appendix.

Introduce the standard diffusion limit scaling in equation (38) using the non-dimensional parameter $0 < \varepsilon \leq 1$,

$$(\Omega^{(d)} \cdot \mathbf{G} + F_d) \boldsymbol{\psi}_d + \varepsilon^{-1} \mathbf{M}_t \boldsymbol{\psi}_d = \frac{1}{4\pi} (\varepsilon^{-1} \mathbf{M}_t - \varepsilon \mathbf{M}_a) \boldsymbol{\phi} + \varepsilon M Q_d, \quad (42)$$

where

$$\boldsymbol{\phi} = \boldsymbol{\beta}^T (\hat{W}^{-1} \boldsymbol{\psi}).$$

Here ε characterizes the photon mean free path relative to the mesh spacing, and $0 < \varepsilon \ll 1$ results in arbitrarily large iteration counts for fixed point iteration of equation (42).

In Section 7.2, we derive the following discrete diffusion approximation,

$$\frac{1}{3} \sum_{j=1}^3 \left(G_j + \bar{F}_j \right)^T \mathbf{M}_t^{-1} \left(G_j + \bar{F}_j \right) \boldsymbol{\phi} + F_0 \boldsymbol{\phi} + M_a \boldsymbol{\phi} \approx M Q^+.$$

Here G_j is defined in equation (41) and \bar{F}_j is defined by

$$\mathbf{v}^T \bar{F}_j \mathbf{u} = \sum_{\Gamma \in F} \int_{\Gamma} [\![u]\!] \{v\} dS,$$

and

$$\mathbf{v}^T F_0 \mathbf{u} = \frac{1}{4\pi} \sum_{\Gamma \in \mathcal{F}} \left(\frac{1}{2} \int_{\Gamma} \boldsymbol{\beta}^T \hat{W}^{-1} \left[\left[\mathbf{\Omega}^{(d)} \cdot \mathbf{n} \right] \right]_{d=1}^r \right) \llbracket u \rrbracket \llbracket v \rrbracket dS. \quad (43)$$

We note that this form is identical to a traditional consistent DSA discretization for DG discretizations of equation (5). The only difference is in the penalty term (43) (cf. [18]); in practice, we have observed that using the penalty term from [18] is sufficient for good acceleration, and we use this version for simplicity in the numerical experiments in Section 5.

5. Numerical experiments

Here we compare the PN-like and SN-like DLR methods against a classic SN TRT solver on two challenging test problems. The test problem in Section 5.1 contains extremely optically thick and optically thin spatial regions, and its efficient solution necessitates implicit time-stepping and—in the SN-like DLR method—carefully designed acceleration methods such as the DSA scheme discussed in Section 4.5. The test problem in Section 5.2 is even more challenging for standard SN methods, due to the point-like radiation sources from the hot spots on the hohlraum wall in to the very thin hohlraum cavity, and the even more severe “ray effects” resulting from the under-resolution in angle.

The spatial discretization we used for the SN-like DLR method is detailed in Section 4.4. For the spatial discretization of the PN-like DLR method, we use a second-order continuous Galerkin finite element discretization. All three methods (the SN, SN-like DLR, and PN-like DLR) use the same spatial meshes, which are displayed in Figures 1 and 3.

Comparing the relative efficiency of the PN-like and SN-like methods is beyond the scope of this paper. However, we do make the following observations. First, we observe that the SN-like DLR method has the same computational performance as the SN method when both use the same number of angles; this results from both using the same highly efficient sweep algorithms and both requiring nearly identical numbers of iterations to converge the implicit solution for each time step. Importantly, we also observe that the SN-like DLR method displays noticeably less angular artifacts from under-resolution than the SN method when both use a comparable number of angles. In contrast, the PN-like DLR method exhibits no ray effects; although it requires two $r_0 \times r_0$ block-diffusion system solves per time step, this cost is likely offset in problems where ray effects are particularly challenging, such as the test problem in Section 5.2. We leave the careful comparison of the relative efficiency of these schemes to future work.

5.1. Lattice problem

We consider a grey version of the problem in [4]. This problem has highly heterogeneous materials—some very optically thick and some very optically thin—and serves as an excellent stress test for numerical TRT methods.

As shown in Figure 1, the lattice problem consists of a checkerboard pattern of materials with very optically thick iron blocks (the light blue-green region corresponds to hot iron and the yellow regions to cold iron), moderately thick blocks of diamond (red regions), and optically thin blocks of foam (blue regions). The mesh elements are chosen to accumulate at material interfaces (see Figure 1).

For simplicity, the opacity of each material is chosen to be fixed instead of temperature dependent; however, realistic opacity values are chosen from the opacity plots in figure 3 in [4]. Specifically, the blocks of iron (light blue-green and yellow blocks) have material opacity $\sigma_a = 10^4 \text{ cm}^{-1}$, specific heat $c_v = 0.05427 \text{ GJ}/(\text{g} \cdot \text{keV})$, and density $\rho = 8.0 \text{ g}/\text{cm}^3$. The blocks of diamond (red blocks) have $\sigma_a = 10^2 \text{ cm}^{-1}$, $c_v = 0.05427 \text{ GJ}/(\text{g} \cdot \text{keV})$, and $\rho = 2.0 \text{ g}/\text{cm}^3$. The blocks of foam (blue blocks) have $\sigma_a = 4 \text{ cm}^{-1}$, $c_v = 0.02412 \text{ GJ}/(\text{g} \cdot \text{keV})$, and $\rho = 0.2 \text{ g}/\text{cm}^3$.

Figure 2 shows the PN-like DLR scheme from Section 3 with rank 8, the SN-like DLR scheme from Section 4 with rank 16, and the S6 scheme (with 36 angles) and S10 scheme (with 100 angles) applied to the lattice problem. Plots Figure 2(a)-(d) show the material temperature at times $t = 3$, $t = 14$, and $t = 25$. As can be seen from the plots, the S6 method (Figure 2(c),(g),(k)) has much more visible “ray effects” from under-resolution in angle than either of the DLR methods. Note that the SN-like DLR method with 16 angles has about the computational cost and memory footprint of the S6 method (by symmetry in xy geometry, we need only solving for half the angles for S6 and S10).

5.2. Hohlraum problem

We consider a hohlraum problem, as shown in Figure 3. Figure 3(a) shows the material regions for the hohlraum problem. The center light blue disc in Figure 3(a) corresponds to the capsule, and has an absorption opacity of

$\sigma_a = 10^2 \text{ cm}^{-1}$, a specific heat of $c_v = 0.05427 \text{ GJ}/(\text{g} \cdot \text{keV})$, and a density of $\rho = 2.0 \text{ g}/\text{cm}^3$. The dark blue region surrounding the capsule corresponds to a foam-filled hohlraum with an absorption opacity of $\sigma_a = 4 \text{ cm}^{-1}$, a specific heat of $c_v = 0.02412 \text{ GJ}/(\text{g} \cdot \text{keV})$, and a density of $\rho = 0.2 \text{ g}/\text{cm}^3$. The red region in Figure 3(a) corresponds to the hohlraum walls and has an absorption opacity of $\sigma_a = 10^4 \text{ cm}^{-1}$, a specific heat of $c_v = 0.05427 \text{ GJ}/(\text{g} \cdot \text{keV})$, and a density of $\rho = 8.0 \text{ g}/\text{cm}^3$. As shown in Figure 3(b), the initial material temperature is $T_{\text{init}} = 0.0001 \text{ keV}$ in the blue regions and $T_{\text{init}} = 0.3 \text{ keV}$ in the eight “hot spots” in the hohlraum walls (shown in the red regions). The hot spots represent where the cones of laser beams entering the hohlraum through the wall openings heat the outer surface of the hohlraum walls.

Figure 4 shows the PN-like DLR scheme from Section 3 with rank 8, the SN-like DLR scheme from Section 4 with rank 16, and the S6 scheme (with 36 angles) applied to the hohlraum problem. Because the point-source-like hot spots on the hohlraum walls radiate into the very optically thin cavity, the ray effects in both the SN-like DLR method and the standard SN method are highly visible; however, the ray effects in the SN-like DLR method appear somewhat mitigated in comparison to the S6 method. In contrast, the PN-like DLR method shows a much smoother behavior in angle.

6. Conclusions

We develop two new types of DLR schemes for TRT. One scheme takes a traditional DLR approach applied to the TRT equations, resulting in a PN-like scheme. The novelty of this method is that it uses an even-parity formulation to allow the time stepping of the method to be done efficiently in the lack of traditional fast transport sweeps. The second method uses a collocation-DLR approach to produce an SN-like DLR scheme. This method has the advantage that it can be adapted to current SN production methods that use state-of-the-art sweep solvers with minimal conversion. In combination with DLR compression, this approach is particularly promising for adoption in application codes.

We demonstrate the two new methods in comparison with a traditional non-DLR TRT SN solver on two challenging test problems. The results show that the methods give solutions of comparable or superior quality to the non-DLR method even at modest rank.

7. Appendix

7.1. Derivation of time-stepping scheme for PN-like DLR method

Assume that

$$\frac{\partial \psi}{\partial t} = \mathcal{L}\psi.$$

Also assume that

$$\begin{aligned} \psi(\mathbf{x}, \boldsymbol{\Omega}, t) &= \sum_{i,j=1}^r X_i(\mathbf{x}, t) S_{ij}(t) W_j(\boldsymbol{\Omega}, t) \\ &= \sum_{j=1}^r K_j(\mathbf{x}, t) W_j(\boldsymbol{\Omega}, t) \\ &= \sum_{i=1}^r X_i(\mathbf{x}, t) L_i(\boldsymbol{\Omega}, t), \end{aligned}$$

where

$$K_j = \sum_{i=1}^r X_i S_{ij}, \quad L_i = \sum_{j=1}^r S_{ij} W_j.$$

Now

$$\frac{\partial \psi}{\partial t} = \sum_{j=1}^r \dot{K}_j W_j + \sum_{j=1}^r K_j \dot{W}_j$$

$$= \sum_{j=1}^r \dot{X}_j L_j + \sum_{j=1}^r X_j \dot{L}_j.$$

Therefore,

$$\dot{L}_j = \left\langle \frac{\partial \psi}{\partial t}, X_j \right\rangle_{\mathcal{X}}, \quad \dot{K}_j = \left\langle \frac{\partial \psi}{\partial t}, W_j \right\rangle_{\mathbb{S}^2}.$$

So for consistency

$$\dot{L}_j = \left\langle \frac{\partial \psi}{\partial t}, X_j \right\rangle_{\mathcal{X}} = \langle \mathcal{L}\psi, X_j \rangle_{\mathcal{X}},$$

and

$$\dot{K}_j = \left\langle \frac{\partial \psi}{\partial t}, W_j \right\rangle_{\mathcal{X}} = \langle \mathcal{L}\psi, W_j \rangle_{\mathcal{X}}.$$

That is, we compute \dot{K}_j, \dot{L}_j from Galerkin conditions

$$\left\langle \frac{\partial \psi}{\partial t} - \mathcal{L}\psi, X_j \right\rangle_{\mathcal{X}} = 0, \quad \left\langle \frac{\partial \psi}{\partial t} - \mathcal{L}\psi, W_j \right\rangle_{\mathbb{S}^2} = 0.$$

Now,

$$\langle \mathcal{L}\psi, X_j \rangle_{\mathcal{X}} = \sum_{i=1}^r \langle \mathcal{L}(X_i L_i), X_j \rangle_{\mathcal{X}},$$

$$\langle \mathcal{L}\psi, W_j \rangle_{\mathcal{X}} = \sum_{i=1}^r \langle \mathcal{L}(W_i K_i), W_j \rangle_{\mathbb{S}^2},$$

and so

$$\dot{L}_j = \sum_{i=1}^r \langle \mathcal{L}(X_i L_i), X_j \rangle_{\mathcal{X}},$$

$$\dot{K}_j = \sum_{i=1}^r \langle \mathcal{L}(W_i K_i), W_j \rangle_{\mathbb{S}^2}.$$

Finally consider

$$\psi(\mathbf{x}, \boldsymbol{\Omega}, t) = \sum_{i,j=1}^r X_i(\mathbf{x}, t) S_{ij}(t) W_j(\boldsymbol{\Omega}, t).$$

Then

$$\frac{\partial \psi}{\partial t} = \sum_{i,j=1}^r \dot{X}_i S_{ij} W_j + \sum_{i,j=1}^r X_i \dot{S}_{ij} W_j + \sum_{i,j=1}^r X_i S_{ij} \dot{W}_j.$$

It follows that

$$\dot{S}_{ij} = \left\langle \frac{\partial \psi}{\partial t}, X_i W_j \right\rangle_{\mathcal{X} \times \mathbb{S}^2} = \langle \mathcal{L}\psi, X_i W_j \rangle_{\mathcal{X} \times \mathbb{S}^2}.$$

Therefore,

$$\begin{aligned}\dot{S}_{ij} &= \left\langle \mathcal{L} \sum_{i',j'=1}^r X_{i'} S_{i'j'} W_{j'}, X_i W_j \right\rangle_{\mathcal{X} \times \mathbb{S}^2} \\ &= \sum_{i',j'=1}^r S_{i'j'} \langle \mathcal{L} X_{i'} W_{j'}, X_i W_j \rangle_{\mathcal{X} \times \mathbb{S}^2}.\end{aligned}$$

In summary,

$$\begin{aligned}\dot{L}_j &= \sum_{i=1}^r \langle \mathcal{L} (X_i L_i), X_j \rangle_{\mathcal{X}}, \\ \dot{K}_j &= \sum_{i=1}^r \langle \mathcal{L} (K_i W_i), W_j \rangle_{\mathbb{S}^2}, \\ \dot{S}_{ij} &= \sum_{i',j'=1}^r S_{i'j'} \langle \mathcal{L} X_{i'} W_{j'}, X_i W_j \rangle_{\mathcal{X} \times \mathbb{S}^2}.\end{aligned}$$

We claim that

$$\frac{\partial \psi}{\partial t} = \sum_j \dot{K}_j W_j + \sum_i \dot{L}_i X_i - \sum_{i,j=1}^r X_i \dot{S}_{ij} W_j.$$

To show this, recall that

$$K_j = \sum_{i=1}^r X_i S_{ij}, \quad L_i = \sum_{j=1}^r S_{ij} W_j.$$

Therefore,

$$\dot{K}_j = \sum_{i=1}^r \dot{X}_i S_{ij} + \sum_{i=1}^r X_i \dot{S}_{ij},$$

and so

$$\sum_j \dot{K}_j W_j = \sum_{i,j=1}^r \dot{X}_i S_{ij} W_j + \sum_{i,j=1}^r X_i \dot{S}_{ij} W_j.$$

Similarly,

$$\dot{L}_i = \sum_{j=1}^r S_{ij} \dot{W}_j + \sum_{i=1}^r \dot{S}_{ij} W_j,$$

and so

$$\sum_i \dot{L}_i X_i = \sum_{i,j=1}^r X_i S_{ij} \dot{W}_j + \sum_{i,j=1}^r X_i \dot{S}_{ij} W_j.$$

It follows that

$$\sum_j \dot{K}_j W_j + \sum_i \dot{L}_i X_i = \sum_{i,j=1}^r \dot{X}_i S_{ij} W_j + 2 \sum_{i,j=1}^r X_i \dot{S}_{ij} W_j + \sum_{i,j=1}^r X_i S_{ij} \dot{W}_j.$$

Therefore,

$$\begin{aligned} \sum_j \dot{K}_j W_j + \sum_i \dot{L}_i X_i - \sum_{i,j=1}^r X_i \dot{S}_{ij} W_j &= \sum_{i,j=1}^r \dot{X}_i S_{ij} W_j + \sum_{i,j=1}^r X_i \dot{S}_{ij} W_j + \sum_{i,j=1}^r X_i S_{ij} \dot{W}_j \\ &= \frac{\partial}{\partial t} \left(\sum_{i,j=1}^r X_i S_{ij} W_j \right). \end{aligned}$$

7.2. Derivation of DSA for collocation-based DLR

7.2.1. Diffusion limit

Write equation (40) as

$$\left(I + \varepsilon \sum_{k=1}^3 \Omega_k M_t^{-1} A_k \right) \mathbf{L} = \frac{1}{4\pi} (I - \varepsilon^2 M_t^{-1} M_a) \int_{\mathbb{S}^2} \mathbf{L} d\Omega + \varepsilon M_t^{-1} \mathbf{Q}.$$

In the diffusion limit,

$$\begin{aligned} \left(I + \varepsilon \sum_{k=1}^3 \Omega_k M_t^{-1} A_k \right)^{-1} &= I - \varepsilon \sum_{k=1}^3 \Omega_k M_t^{-1} A_k + \\ &\quad \varepsilon^2 \left(\sum_{k=1}^3 \Omega_k M_t^{-1} A_k \right)^2 + \mathcal{O}(\varepsilon^3). \end{aligned}$$

To order $\mathcal{O}(\varepsilon^2)$, $L_j(\Omega)$ can be written as linear combinations of 1, Ω_k , $\Omega_k \Omega_l$,

$$L_j(\Omega) = a_j + \sum_{k=1}^3 a_{j,k} \Omega_k + \sum_{k,l=1}^3 a_{j,k,l} \Omega_k \Omega_l + \mathcal{O}(\varepsilon^3).$$

It follows that there are coefficients $b_{d'}$, $b_{d',k}$, $b_{d',k,l}$ for which

$$W_{d'}(\Omega) = b_{d'} + \sum_{k=1}^3 b_{d',k}(\Omega)_k + \sum_{k,l=1}^3 b_{d',k,l}(\Omega)_k(\Omega)_l + \mathcal{O}(\varepsilon^3), \quad d' = 1, \dots, r_0. \quad (44)$$

Assume that we can solve, up to errors of order $\mathcal{O}(\varepsilon^3)$, equations (44) for the basis functions 1, $(\Omega)_k(\Omega)_l$, $(\Omega)_k(\Omega)_l$, $k, l = 1, 2, 3$, in terms of $W_{d'}(\Omega)$, $d' = 1, \dots, r_0$. Then there are coefficients $\alpha_{d'}^{(i,j)}$ for which

$$(\Omega)_i(\Omega)_j = \sum_{d'=1}^{r_0} \alpha_{d'}^{(i,j)} W_{d'}(\Omega) + \mathcal{O}(\varepsilon^3).$$

Therefore,

$$(\Omega_d)_i(\Omega_d)_j = \sum_{d'=1}^{r_0} \alpha_{d'}^{(i,j)} W_{d'}(\Omega_d) + \mathcal{O}(\varepsilon^3), \quad d = 1, \dots, r_0.$$

It follows that, for each $i, j = 1, 2, 3$,

$$\boldsymbol{\alpha}^{(i,j)} = \hat{W}^{-1} \left[(\Omega_d)_i(\Omega_d)_j \right]_{d=1}^{r_0} + \mathcal{O}(\varepsilon^3).$$

We then calculate that

$$\begin{aligned} \int_{\mathbb{S}^2} (\Omega)_i(\Omega)_j d\Omega &= \sum_{d'} \alpha_{d'}^{(i,j)} \int_{\mathbb{S}^2} W_{d'}(\Omega) d\Omega + \mathcal{O}(\varepsilon^3) \\ &= \boldsymbol{\beta}^T \boldsymbol{\alpha}^{(i,j)} + \mathcal{O}(\varepsilon^3) \\ &= \boldsymbol{\beta}^T \hat{W}^{-1} \left[(\Omega_d)_i(\Omega_d)_j \right]_{d=1}^r + \mathcal{O}(\varepsilon^3). \end{aligned}$$

7.2.2. Diffusion Synthetic Acceleration (DSA) for SN-like DLR method

Recall that

$$(\boldsymbol{\Omega}_d \cdot \mathbf{G} + F_d) \boldsymbol{\psi}_d + M_t \boldsymbol{\psi}_d = \frac{M_s}{4\pi} \boldsymbol{\phi} + M Q_d,$$

$$\boldsymbol{\phi} = \boldsymbol{\beta}^T (\hat{W}^{-1} \boldsymbol{\psi}).$$

Here $\hat{W} = [W_i(\boldsymbol{\Omega}_j)]_{i,j=1}^r$, $\beta_i = \int_{\mathbb{S}^2} W_i(\boldsymbol{\Omega}) d\boldsymbol{\Omega}$, and

$$\begin{aligned} \mathbf{v}^T F_d \mathbf{u} &= - \sum_{\Gamma \in \mathcal{F}} \int_{\Gamma} \boldsymbol{\Omega}_d \cdot \mathbf{n} [\![u]\!] \{v\} dS + \frac{1}{2} \sum_{\Gamma \in \mathcal{F}} \int_{\Gamma} |\boldsymbol{\Omega}_d \cdot \mathbf{n}| [\![u]\!] [\![v]\!] dS \\ &= \mathbf{v}^T (\boldsymbol{\Omega}_d \cdot \mathbf{F}) \mathbf{u} + \mathbf{v}^T F_d^{\parallel\parallel} \mathbf{u}. \end{aligned}$$

Let $\hat{\boldsymbol{\psi}}_d$ denote the solution to

$$(-\boldsymbol{\Omega}_d \cdot \mathbf{G} + F_d) \hat{\boldsymbol{\psi}}_d + M_t \boldsymbol{\psi}_d = \frac{M_s}{4\pi} \boldsymbol{\phi} + M Q_d,$$

$$\boldsymbol{\phi} = \boldsymbol{\beta}^T (\hat{W}^{-1} \boldsymbol{\psi}).$$

Here

$$\begin{aligned} \mathbf{v}^T F_d \mathbf{u} &= - \sum_{\Gamma \in \mathcal{F}} \int_{\Gamma} \boldsymbol{\Omega}_d \cdot \mathbf{n} [\![u]\!] \{v\} dS + \frac{1}{2} \sum_{\Gamma \in \mathcal{F}} \int_{\Gamma} |\boldsymbol{\Omega}_d \cdot \mathbf{n}| [\![u]\!] [\![v]\!] dS \\ &= \mathbf{v}^T (\boldsymbol{\Omega}_d \cdot \mathbf{F}) \mathbf{u} + \mathbf{v}^T F_d^{\parallel\parallel} \mathbf{u}. \end{aligned}$$

Now,

$$\begin{aligned} \mathbf{v}^T F_{\mathcal{R}(d)} \mathbf{u} &= - \sum_{\Gamma \in \mathcal{F}} \int_{\Gamma} \boldsymbol{\Omega}_{\mathcal{R}(d)} \cdot \mathbf{n} [\![u]\!] \{v\} dS + \frac{1}{2} \sum_{\Gamma \in \mathcal{F}} \int_{\Gamma} |\boldsymbol{\Omega}_{\mathcal{R}(d)} \cdot \mathbf{n}| [\![u]\!] [\![v]\!] dS \\ &= -\mathbf{v}^T (\boldsymbol{\Omega}_d \cdot \mathbf{F}) \mathbf{u} + \mathbf{v}^T F_d^{\parallel\parallel} \mathbf{u}. \end{aligned}$$

It follows that

$$F_{\mathcal{R}(d)} \boldsymbol{\psi}_{\mathcal{R}(d)} = -(\boldsymbol{\Omega}_d \cdot \mathbf{F}) \boldsymbol{\psi}_{\mathcal{R}(d)} + F_d^{\parallel\parallel} \boldsymbol{\psi}_{\mathcal{R}(d)},$$

$$F_d \boldsymbol{\psi}_d = (\boldsymbol{\Omega}_d \cdot \mathbf{F}) \boldsymbol{\psi}_d + F_d^{\parallel\parallel} \boldsymbol{\psi}_d.$$

Now, define

$$\boldsymbol{\psi}_d^+ = \frac{\boldsymbol{\psi}_{\mathcal{R}(d)} + \boldsymbol{\psi}_d}{2}, \quad \boldsymbol{\psi}_d^- = \frac{\boldsymbol{\psi}_d - \boldsymbol{\psi}_{\mathcal{R}(d)}}{2}.$$

We compute that

$$\frac{1}{2} (F_{\mathcal{R}(d)} \boldsymbol{\psi}_{\mathcal{R}(d)} + F_d \boldsymbol{\psi}_d) = (\boldsymbol{\Omega}_d \cdot \mathbf{F}) \boldsymbol{\psi}_d^- + F_d^{\parallel\parallel} \boldsymbol{\psi}_d^+,$$

$$\frac{1}{2} (F_d \boldsymbol{\psi}_d - F_{\mathcal{R}(d)} \boldsymbol{\psi}_{\mathcal{R}(d)}) = (\boldsymbol{\Omega}_d \cdot \mathbf{F}) \boldsymbol{\psi}_d^+ + F_d^{\parallel\parallel} \boldsymbol{\psi}_d^-.$$

Now,

$$(-\boldsymbol{\Omega}_d \cdot \mathbf{G} + F_{\mathcal{R}(d)}) \boldsymbol{\psi}_{\mathcal{R}(d)} + M_t \boldsymbol{\psi}_{\mathcal{R}(d)} = \frac{M_s}{4\pi} \boldsymbol{\phi} + M Q_{\mathcal{R}(d)}.$$

$$(\boldsymbol{\Omega}_d \cdot \mathbf{G} + F_d) \boldsymbol{\psi}_d + M_t \boldsymbol{\psi}_d = \frac{M_s}{4\pi} \boldsymbol{\phi} + M Q_d.$$

Add and subtract these equations and divide by 2:

$$\boldsymbol{\Omega}_d \cdot (\mathbf{G} + \mathbf{F}) \boldsymbol{\psi}_d^- + F_d^{\parallel\parallel} \boldsymbol{\psi}_d^+ + M_t \boldsymbol{\psi}_d^+ = \frac{M_s}{4\pi} \boldsymbol{\phi} + M Q_d^+,$$

$$\boldsymbol{\Omega}_d \cdot (\mathbf{G} + \mathbf{F}) \boldsymbol{\psi}_d^+ + F_d^{\parallel\parallel} \boldsymbol{\psi}_d^- + M_t \boldsymbol{\psi}_d^- = M Q_d^-.$$

Now, define

$$\mathbf{v}^T \tilde{F}_d \mathbf{u} = \sum_{\Gamma \in \mathcal{F}} \int_{\Gamma} \boldsymbol{\Omega}_d \cdot \mathbf{n} [\![v]\!] \{u\} dS + \frac{1}{2} \sum_{\Gamma \in \mathcal{F}} \int_{\Gamma} |\boldsymbol{\Omega}_d \cdot \mathbf{n}| [\![u]\!] [\![v]\!] dS.$$

It turns out that

$$\boldsymbol{\Omega}_d \cdot \mathbf{G} + F_d = -\boldsymbol{\Omega}_d \cdot \mathbf{G}^T + \tilde{F}_d.$$

Recall that

$$\begin{aligned} \mathbf{v}^T F_d \mathbf{u} &= - \sum_{\Gamma \in \mathcal{F}} \int_{\Gamma} \boldsymbol{\Omega}_d \cdot \mathbf{n} [\![u]\!] \{v\} dS + \frac{1}{2} \sum_{\Gamma \in \mathcal{F}} \int_{\Gamma} |\boldsymbol{\Omega}_d \cdot \mathbf{n}| [\![u]\!] [\![v]\!] dS \\ &= \mathbf{v}^T (\boldsymbol{\Omega}_d \cdot \mathbf{F}) \mathbf{u} + \mathbf{v}^T F_d^{\parallel\parallel} \mathbf{u}. \end{aligned}$$

Also,

$$\tilde{F}_d = -\boldsymbol{\Omega}_d \cdot \mathbf{F}^T + F_d^{\parallel\parallel}.$$

It follows that

$$\boldsymbol{\Omega}_d \cdot \mathbf{G} + \boldsymbol{\Omega}_d \cdot \mathbf{F} + F_d^{\parallel\parallel} = -\boldsymbol{\Omega}_d \cdot \mathbf{G}^T - \boldsymbol{\Omega}_d \cdot \mathbf{F}^T + F_d^{\parallel\parallel}.$$

Therefore, we obtain the equations for the even and odd components,

$$-\boldsymbol{\Omega}_d \cdot (\mathbf{G} + \mathbf{F})^T \boldsymbol{\psi}_d^- + F_d^{\parallel\parallel} \boldsymbol{\psi}_d^+ + M_t \boldsymbol{\psi}_d^+ = \frac{M_s}{4\pi} \boldsymbol{\phi} + M Q_d^+,$$

$$\boldsymbol{\Omega}_d \cdot (\mathbf{G} + \mathbf{F}) \boldsymbol{\psi}_d^+ + F_d^{\parallel\parallel} \boldsymbol{\psi}_d^- + M_t \boldsymbol{\psi}_d^- = M Q_d^-.$$

Now,

$$\begin{aligned} \boldsymbol{\psi}_d^- &= \left(I + M_t^{-1} F_d^{\parallel\parallel} \right)^{-1} M_t^{-1} (M Q_d^-) - \left(I + M_t^{-1} F_d^{\parallel\parallel} \right)^{-1} M_t^{-1} \boldsymbol{\Omega}_d \cdot (\mathbf{G} + \mathbf{F}) \boldsymbol{\psi}_d^+ \\ &= -M_t^{-1} \boldsymbol{\Omega}_d \cdot (\mathbf{G} + \mathbf{F}) \boldsymbol{\psi}_d^+ + M_t^{-1} (M Q_d^-) + \\ &\quad \left(\left(I + M_t^{-1} F_d^{\parallel\parallel} \right)^{-1} - I \right) M_t^{-1} (M Q_d^-) - \\ &\quad \left(\left(I + M_t^{-1} F_d^{\parallel\parallel} \right)^{-1} - I \right) M_t^{-1} \boldsymbol{\Omega}_d \cdot (\mathbf{G} + \mathbf{F}) \boldsymbol{\psi}_d^+. \end{aligned}$$

Therefore, to leading order

$$\begin{aligned} -\boldsymbol{\Omega}_d \cdot (\mathbf{G} + \mathbf{F})^T (-M_t^{-1} \boldsymbol{\Omega}_d \cdot (\mathbf{G} + \mathbf{F}) \boldsymbol{\psi}_d^+) + F_d^{\parallel\parallel} \boldsymbol{\psi}_d^+ + M_t \boldsymbol{\psi}_d^+ &\approx \frac{M_s}{4\pi} \boldsymbol{\phi} + M Q_d^+ + \\ \boldsymbol{\Omega}_d \cdot (\mathbf{G} + \mathbf{F})^T M_t^{-1} (M Q_d^-) &. \end{aligned}$$

Also, to leading order,

$$\boldsymbol{\psi}_d = M_t^{-1} \frac{M_s}{4\pi} \boldsymbol{\phi} + \mathcal{O}(\varepsilon) = \frac{1}{4\pi} \boldsymbol{\phi} + \mathcal{O}(\varepsilon),$$

and so

$$\boldsymbol{\psi}_d^+ = \frac{1}{4\pi} \boldsymbol{\phi} + \mathcal{O}(\varepsilon), \quad \boldsymbol{\psi}_d^- = \mathcal{O}(\varepsilon).$$

We can drop the term $\boldsymbol{\Omega}_d \cdot (\mathbf{G} + \mathbf{F})^T M_t^{-1} (M Q_d^-)$ since we assume that $Q_d = \mathcal{O}(\varepsilon)$. It follows that

$$-\boldsymbol{\Omega}_d \cdot (\mathbf{G} + \mathbf{F})^T \left(-M_t^{-1} \boldsymbol{\Omega}_d \cdot (\mathbf{G} + \mathbf{F}) \frac{1}{4\pi} \boldsymbol{\phi} \right) + F_d^T \frac{1}{4\pi} \boldsymbol{\phi} + M_t \frac{1}{4\pi} \boldsymbol{\phi} \approx \frac{M_s}{4\pi} \boldsymbol{\phi} + M Q_d^+. \quad (45)$$

Now consider

$$-\boldsymbol{\Omega}_d \cdot (\mathbf{G} + \mathbf{F})^T \left(-M_t^{-1} \boldsymbol{\Omega}_d \cdot (\mathbf{G} + \mathbf{F}) \frac{1}{4\pi} \boldsymbol{\phi} \right) + F_d^T \frac{1}{4\pi} \boldsymbol{\phi} + M_a \frac{1}{4\pi} \boldsymbol{\phi} \approx M Q_d^+.$$

Define

$$\boldsymbol{\alpha} = \hat{W}^{-1} [1]_{d=1}^r,$$

$$\boldsymbol{\alpha}^{(i,j)} = \hat{W}^{-1} \left[(\boldsymbol{\Omega}_d)_i (\boldsymbol{\Omega}_d)_j \right]_{d=1}^r,$$

$$\gamma = \boldsymbol{\beta}^T \boldsymbol{\alpha},$$

$$\gamma^{(i,j)} = \boldsymbol{\beta}^T \boldsymbol{\alpha}^{(i,j)}.$$

Let

$$\tilde{\boldsymbol{\phi}}_d = (\boldsymbol{\Omega}_d)_i (\boldsymbol{\Omega}_d)_j (\mathbf{G}_i + \mathbf{F}_i)^T M_t^{-1} (\mathbf{G}_j + \mathbf{F}_j) \boldsymbol{\phi}.$$

Then

$$\begin{aligned} \boldsymbol{\beta}^T \hat{W}^{-1} [\tilde{\boldsymbol{\phi}}_d]_d &= \boldsymbol{\beta}^T \hat{W}^{-1} \left[(\boldsymbol{\Omega}_d)_i (\boldsymbol{\Omega}_d)_j \right]_{d=1}^r (\mathbf{G}_i + \mathbf{F}_i)^T M_t^{-1} (\mathbf{G}_j + \mathbf{F}_j) \boldsymbol{\phi} \\ &= \boldsymbol{\beta}^T \boldsymbol{\alpha}^{(i,j)} (\mathbf{G}_i + \mathbf{F}_i)^T M_t^{-1} (\mathbf{G}_j + \mathbf{F}_j) \boldsymbol{\phi}. \end{aligned}$$

It follows that the DSA matrix can be written as

$$\sum_{i,j=1}^3 \gamma^{(i,j)} (\mathbf{G}_i + \mathbf{F}_i)^T M_t^{-1} (\mathbf{G}_j + \mathbf{F}_j) \boldsymbol{\phi} + F_0 \frac{1}{4\pi} \boldsymbol{\phi} + \gamma M_a \frac{1}{4\pi} \boldsymbol{\phi}.$$

Here

$$\mathbf{v}^T F_0 \mathbf{u} = \frac{1}{4\pi} \sum_{\Gamma \in \mathcal{F}} \left(\frac{1}{2} \int_{\Gamma} \boldsymbol{\beta}^T \hat{W}^{-1} [|\boldsymbol{\Omega}_d \cdot \mathbf{n}|]_{d=1}^r \right) [u] [v] dS.$$

Now, suppose that

$$(\boldsymbol{\Omega}_d)_i (\boldsymbol{\Omega}_d)_j = \sum_{d'=1}^{r'} \alpha_{d'}^{(i,j)} W_{d'} (\boldsymbol{\Omega}_d),$$

so that

$$\boldsymbol{\alpha}^{(i,j)} = \hat{W}^{-1} \left[(\boldsymbol{\Omega}_d)_i (\boldsymbol{\Omega}_d)_j \right]_{d=1}^r.$$

Also,

$$\int_{\mathbb{S}^2} (\boldsymbol{\Omega})_i (\boldsymbol{\Omega})_j d\boldsymbol{\Omega} = \sum_{d'} \alpha_{d'}^{(i,j)} \int_{\mathbb{S}^2} W_{d'} (\boldsymbol{\Omega}) d\boldsymbol{\Omega} = \boldsymbol{\beta}^T \boldsymbol{\alpha}^{(i,j)} = \boldsymbol{\beta}^T \hat{W}^{-1} \left[(\boldsymbol{\Omega}_d)_i (\boldsymbol{\Omega}_d)_j \right]_{d=1}^r.$$

Now,

$$\boldsymbol{\Omega}_d \cdot (\mathbf{G} + \mathbf{F})^T M_t^{-1} \boldsymbol{\Omega}_d \cdot (\mathbf{G} + \mathbf{F}) = \sum_{i,j=1}^3 (\boldsymbol{\Omega}_d)_i (\boldsymbol{\Omega}_d)_j (\mathbf{G}_i + \mathbf{F}_i)^T M_t^{-1} (\mathbf{G}_j + \mathbf{F}_j).$$

Let

$$\tilde{\boldsymbol{\phi}}_d = (\boldsymbol{\Omega}_d)_i (\boldsymbol{\Omega}_d)_j (\mathbf{G}_i + \mathbf{F}_i)^T M_t^{-1} (\mathbf{G}_j + \mathbf{F}_j) \boldsymbol{\phi}.$$

Then

$$\begin{aligned} \boldsymbol{\beta}^T \hat{W}^{-1} [\tilde{\boldsymbol{\phi}}_d]_d &= \boldsymbol{\beta}^T \hat{W}^{-1} \left[(\boldsymbol{\Omega}_d)_i (\boldsymbol{\Omega}_d)_j \right]_{d=1}^r (\mathbf{G}_i + \mathbf{F}_i)^T M_t^{-1} (\mathbf{G}_j + \mathbf{F}_j) \boldsymbol{\phi} \\ &= \left(\int_{\mathbb{S}^2} (\boldsymbol{\Omega})_i (\boldsymbol{\Omega})_j d\boldsymbol{\Omega} \right) (\mathbf{G}_i + \mathbf{F}_i)^T M_t^{-1} (\mathbf{G}_j + \mathbf{F}_j) \boldsymbol{\phi} \\ &= \frac{4\pi}{3} \delta_{i,j} (\mathbf{G}_i + \mathbf{F}_i)^T M_t^{-1} (\mathbf{G}_j + \mathbf{F}_j) \boldsymbol{\phi}. \end{aligned}$$

Applying $\boldsymbol{\beta}^T \hat{W}^{-1}$ to equation (45), it follows that

$$\frac{1}{3} (\mathbf{G} + \mathbf{F})^T M_t^{-1} \cdot (\mathbf{G} + \mathbf{F}) \boldsymbol{\phi} + F_0 \boldsymbol{\phi} + M_a \boldsymbol{\phi} \approx M Q^+.$$

Here

$$\mathbf{v}^T F_0 \mathbf{u} = \frac{1}{4\pi} \sum_{\Gamma \in F} \left(\frac{1}{2} \int_{\Gamma} \boldsymbol{\beta}^T \hat{W}^{-1} [|\boldsymbol{\Omega}_d \cdot \mathbf{n}|]_{d=1}^r \right) [u] [v] dS.$$

We also used that

$$\begin{aligned} \boldsymbol{\beta}^T \hat{W}^{-1} [1]_{d=1}^r &= 4\pi + \mathcal{O}(\varepsilon), \\ \boldsymbol{\beta}^T \hat{W}^{-1} \left[(\boldsymbol{\Omega}_d)_i (\boldsymbol{\Omega}_d)_j \right]_{d=1}^r &= \int_{\mathbb{S}^2} (\boldsymbol{\Omega})_i (\boldsymbol{\Omega})_j d\boldsymbol{\Omega} + \mathcal{O}(\varepsilon). \end{aligned}$$

8. Acknowledgements

This work was performed under the auspices of the U.S. Department of Energy by Lawrence Livermore National Laboratory under Contract DE-AC52-07NA27344. This material is based upon work supported by the U.S. Department of Energy, Office of Science, Office of Mathematical Multifaceted Integrated Capability Center (MMICC) under Award Number DE-SC-000XXXX.

This work has been reviewed for unlimited public release as LLNL-JRNL-2015102.

References

- [1] SJ Aarseth, JU Brackbill, and BI Cohen. Multiple time scales. In *Methods for N-body Simulations*, pages 377–418. Academic Press New York, 1985.
- [2] Marvin L. Adams and Edward W. Larsen. Fast iterative methods for discrete-ordinates particle transport calculations. *Progress in Nuclear Energy*, 40(1):3–159, 2002.
- [3] Lena Baumann, Lukas Einkemmer, Christian Klingenberg, and Jonas Kusch. Energy stable and conservative dynamical low-rank approximation for the Su-Olson problem. 2023.
- [4] Thomas A Brunner. A family of multi-dimensional thermal radiative transfer test problems. Technical report, Lawrence Livermore National Laboratory (LLNL), Livermore, CA (United States), 2023.
- [5] John I Castor. *Radiation hydrodynamics*. 2004.
- [6] G. Ceruti, J. Kusch, and C. Lubich. A Parallel Rank-Adaptive Integrator for Dynamical Low-Rank Approximation. *SIAM J. Sci. Comput.*, 46(3):B205–B228, 2024.

- [7] S Dargaville, RP Smedley-Stevenson, PN Smith, and CC Pain. Air multigrid with gmres polynomials (airg) and additive preconditioners for boltzmann transport. *Journal of Computational Physics*, 518:113342, 2024.
- [8] Steven Dargaville, Richard Smedley-Stevenson, Paul Smith, and Christopher C Pain. Coarsening and parallelism with reduction multigrids for hyperbolic boltzmann transport. *The International Journal of High Performance Computing Applications*, 39(3):364–384, 2025.
- [9] Alec Dektor. Collocation methods for nonlinear differential equations on low-rank manifolds. *Linear Algebra and its Applications*, 705:143–184, 2025.
- [10] Alec Dektor and Lukas Einkemmer. Interpolatory dynamical low-rank approximation for the 3+ 3d boltzmann-bhgk equation. *arXiv preprint arXiv:2411.15990*, 2024.
- [11] L. Einkemmer and I. Joseph. A mass, momentum, and energy conservative dynamical low-rank scheme for the Vlasov equation. *J. Comput. Phys.*, 443:110495, 2021.
- [12] Lukas Einkemmer, Katharina Kormann, Jonas Kusch, Ryan G. McClaren, and Jing-Mei Qiu. A review of low-rank methods for time-dependent kinetic simulations. *Journal of Computational Physics*, 538:114191, 2025.
- [13] Lukas Einkemmer, Jonas Kusch, and Steffen Schottländer. Construction of high-order conservative basis-update and galerkin dynamical low-rank integrators. *arXiv:2311.06399*, November 2023.
- [14] Lukas Einkemmer and Christian Lubich. A low-rank projector-splitting integrator for the vlasov–poisson equation. *SIAM Journal on Scientific Computing*, 40(5):B1330–B1360, 2018.
- [15] Martin Frank, Jonas Kusch, and Chinmay Patwardhan. Asymptotic-preserving and energy stable dynamical low-rank approximation for thermal radiative transfer equations. *Multiscale Modeling & Simulation*, 23(1):278–312, 2025.
- [16] Behzad Ghahremani and Hessam Babaee. A deim tucker tensor cross algorithm and its application to dynamical low-rank approximation. *Computer Methods in Applied Mechanics and Engineering*, 423:116879, 2024.
- [17] Joshua Hanophy, Ben S. Southworth, Ruipeng Li, Tom Manteuffel, and Jim Morel. Parallel approximate ideal restriction multigrid for solving the sn transport equations. *Nuclear Science and Engineering*, 194(11):989–1008, 2020.
- [18] Terry S. Haut, Ben S. Southworth, Peter G. Maginot, and Vladimir Z. Tomov. Diffusion synthetic acceleration preconditioning for discontinuous galerkin discretizations of $\$s_n\$$ transport on high-order curved meshes. *SIAM Journal on Scientific Computing*, 42(5):B1271–B1301, 2020.
- [19] Othmar Koch and Christian Lubich. Dynamical low-rank approximation. *SIAM Journal on Matrix Analysis and Applications*, 29(2):434–454, 2007.
- [20] H. J. Kopp. Synthetic method solution of the transport equation*. *Nuclear Science and Engineering*, 17(1):65–74, 1963.
- [21] Edward W. Larsen. Diffusion-synthetic acceleration methods for discrete-ordinates problems. *Transport Theory and Statistical Physics*, 13(1-2):107–126, 1984.
- [22] V.I. Lebedev. Convergence of the kp-method for some neutron transfer problems. *USSR Computational Mathematics and Mathematical Physics*, 9(1):309–323, 1969.
- [23] EE Lewis. Progress in multidimensional neutron transport computation. *Nuclear Science and Engineering*, 64(2):279–293, 1977.
- [24] William McLendon III, Bruce Hendrickson, Steve Plimpton, and Lawrence Rauchwerger. Finding strongly connected components in parallel in particle transport sweeps. In *Proceedings of the thirteenth annual ACM symposium on Parallel algorithms and architectures*, pages 328–329, 2001.
- [25] Mohammad Hossein Naderi, Sara Akhavan, and Hessam Babaee. A cross algorithm for implicit time integration of random partial differential equations on low-rank matrix manifolds. *Proceedings of the Royal Society A: Mathematical, Physical and Engineering Sciences*, 481(2309):20240658, 03 2025.
- [26] Shawn D Pautz. An algorithm for parallel sn sweeps on unstructured meshes. *Nuclear Science and Engineering*, 140(2):111–136, 2002.
- [27] Shawn D Pautz and Teresa S Bailey. Parallel deterministic transport sweeps of structured and unstructured meshes with overloaded mesh decompositions. *Nuclear Science and Engineering*, 185(1):70–77, 2017.
- [28] Zhuogang Peng and Ryan G McClaren. A high-order/low-order (holo) algorithm for preserving conservation in time-dependent low-rank transport calculations. *Journal of Computational Physics*, 447:110672, 2021.
- [29] Zhuogang Peng and Ryan G McClaren. A low-rank method for the discrete ordinate transport equation compatible with transport sweeps. In *Proceedings of the international conference on mathematics and computational methods applied to nuclear science and engineering-M and C 2021*, pages 1258–1267, 2021.
- [30] Zhuogang Peng and Ryan G McClaren. A sweep-based low-rank method for the discrete ordinate transport equation. *Journal of Computational Physics*, 473:111748, 2023.
- [31] Zhuogang Peng, Ryan G McClaren, and Martin Frank. A low-rank method for two-dimensional time-dependent radiation transport calculations. *Journal of Computational Physics*, 421:109735, 2020.
- [32] Steven J Plimpton, Bruce Hendrickson, Shawn P Burns, William McLendon III, and Lawrence Rauchwerger. Parallel sn sweeps on unstructured grids: Algorithms for prioritization, grid partitioning, and cycle detection. *Nuclear science and engineering*, 150(3):267–283, 2005.
- [33] Nanyi Zheng, Daniel Hayes, Andrew Christlieb, and Jing-Mei Qiu. A semi-lagrangian adaptive-rank (slar) method for linear advection and nonlinear vlasov-poisson system. *Journal of Computational Physics*, 532:113970, 2025.

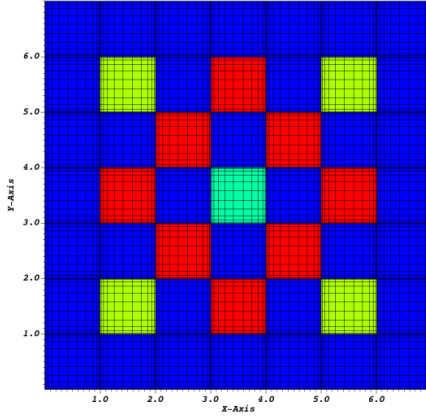


Figure 1: Mesh and materials for the lattice problem defined in [4]. The blue-green block in the center of the spatial domain corresponds to hot iron; the red blocks correspond to diamond; the yellow blocks correspond to cold iron; and the blue blocks correspond to foam.

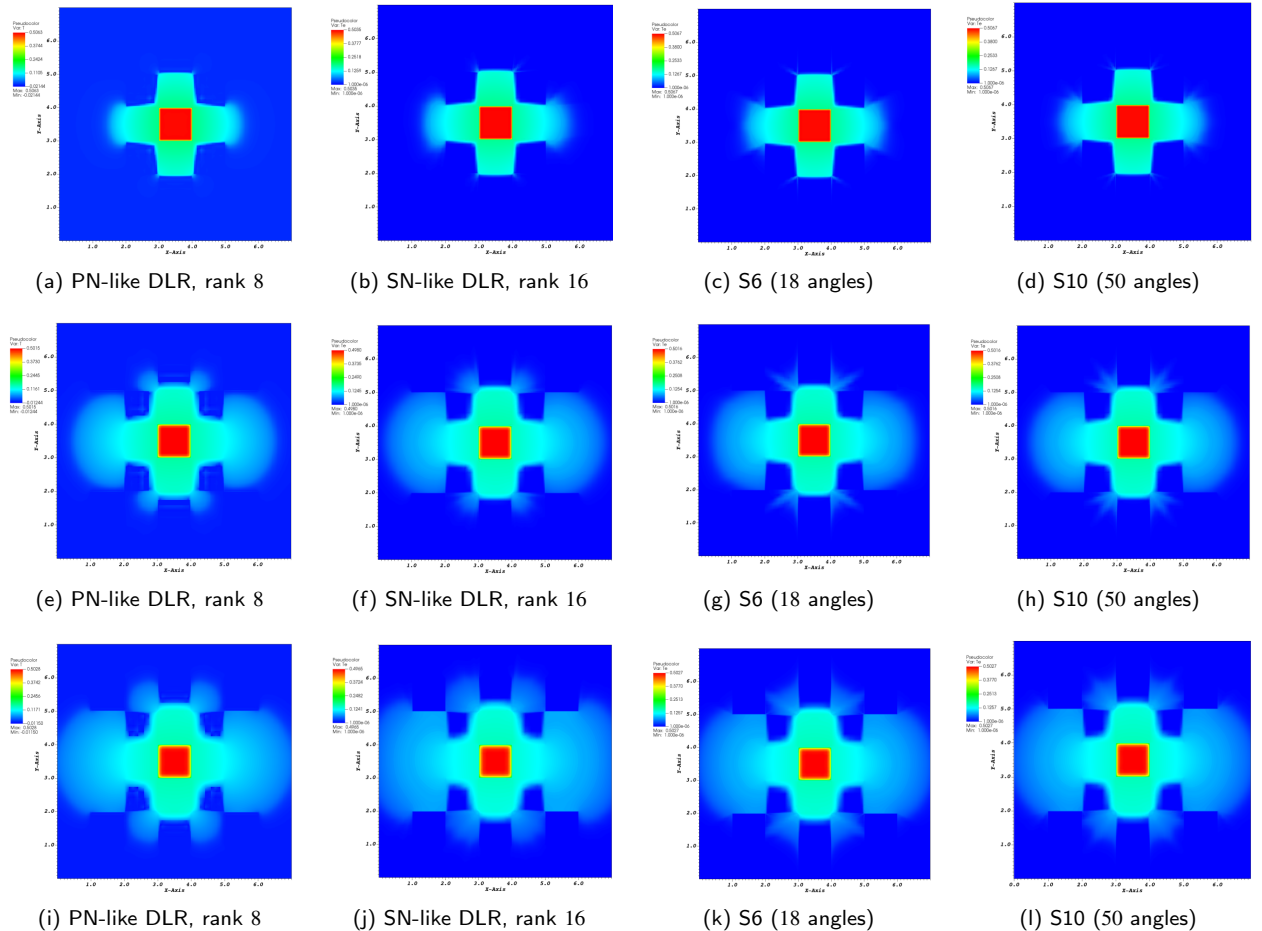


Figure 2: PN-like DLR method with rank 8, SN-like DLR method with rank 16, S6 (18 angles), and S10 (50 angles) for the lattice problem. Material temperature at times $t = 3$, $t = 14$, and $t = 25$.

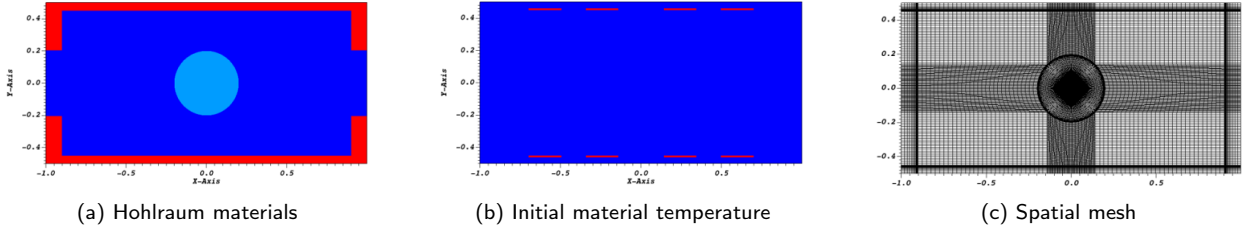
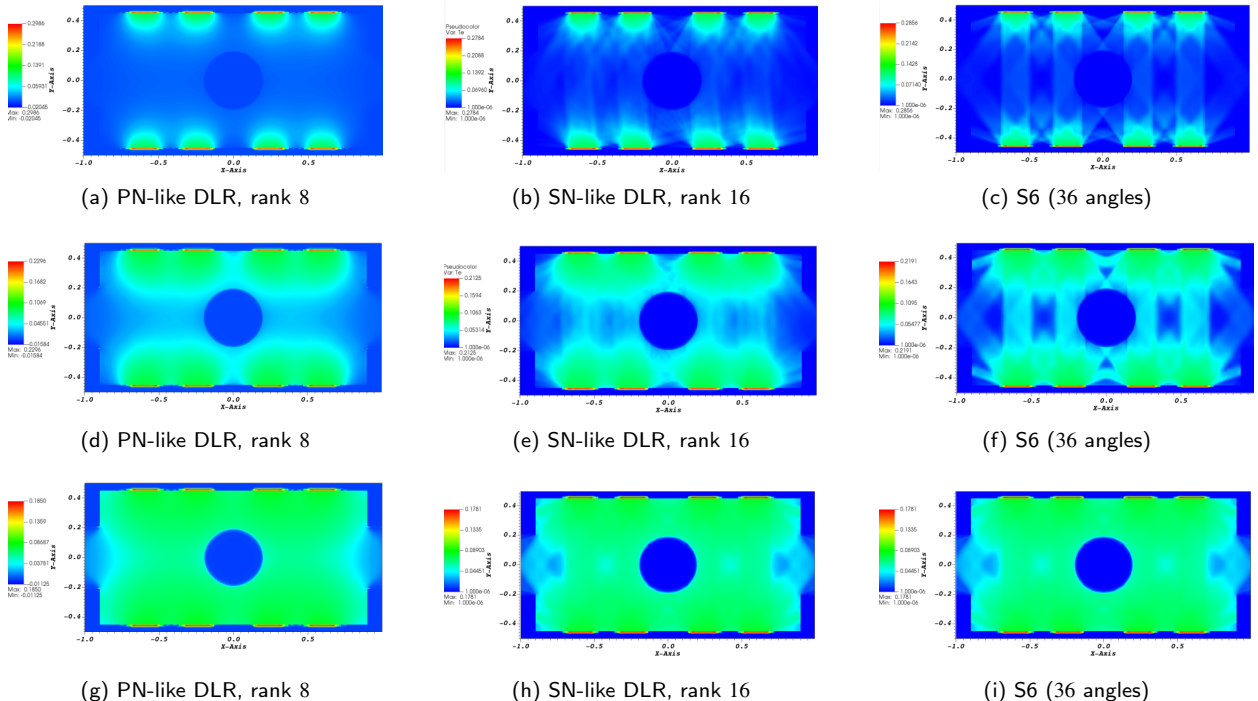


Figure 3: Material regions, mesh, and initial conditions for the hohlraum problem.

Figure 4: PN-like DLR method with rank 8, SN-like DLR method with rank 16, and S6 (36 angles) for the hohlraum problem. Plots show the material temperature at times $t = 0.3$, $t = 1.2$, and $t = 3.0$.